OXFORD GENETICS

Imaginal disk growth factors are *Drosophila* chitinase-like proteins with roles in morphogenesis and CO₂ response

Anne E. Sustar [1] Liesl G. Strand [1,2] Sandra G. Zimmerman [1,*] Celeste A. Berg [1,*]

[1]Department of Genome Sciences, University of Washington, Foege Bldg. S-250, 3720 15th Ave NE, Seattle, WA 98195-5065, USA
[2]Present address: Department of Developmental Biology, Beckman Center, 279 W. Campus Drive, B300, Stanford University, Stanford, California 94305-5329, USA

*Corresponding author: Email: caberg@uw.edu; *Corresponding author: Email: sgzim@uw.edu

Abstract

Chitinase-like proteins (CLPs) are members of the family 18 glycosyl hydrolases, which include chitinases and the enzymatically inactive CLPs. A mutation in the enzyme's catalytic site, conserved in vertebrates and invertebrates, allowed CLPs to evolve independently with functions that do not require chitinase activity. CLPs normally function during inflammatory responses, wound healing, and host defense, but when they persist at excessive levels at sites of chronic inflammation and in tissue-remodeling disorders, they correlate positively with disease progression and poor prognosis. Little is known, however, about their physiological function. *Drosophila melanogaster* has 6 CLPs, termed Imaginal disk growth factors (Idgfs), encoded by *Idgf1*, *Idgf2*, *Idgf3*, *Idgf4*, *Idgf5*, and *Idgf6*. In this study, we developed tools to facilitate characterization of the physiological roles of the Idgfs by deleting each of the *Idgf* genes using the CRISPR/Cas9 system and assessing loss-of-function phenotypes. Using null lines, we showed that loss of function for all 6 Idgf proteins significantly lowers viability and fertility. We also showed that Idgfs play roles in epithelial morphogenesis, maintaining proper epithelial architecture and cell shape, regulating E-cadherin and cortical actin, and remarkably, protecting these tissues against CO₂ exposure. Defining the normal molecular mechanisms of CLPs is a key to understanding how deviations tip the balance from a physiological to a pathological state.

Keywords: imaginal disk growth factors, chitinase-like proteins, CO₂ exposure, morphogenesis, cell migration, fertility, *Drosophila*, hypercapnia

Introduction

Chitinase-like proteins (CLPs) are secreted glycoproteins with properties of cytokines and growth factors (Kawamura *et al.* 1999; Kzhyshkowska *et al.* 2016; Guan *et al.* 2020; Lu *et al.* 2022). Normally, CLPs aid in inflammatory responses, wound healing, and defense against parasites, but they also have a dark side (Sutherland *et al.* 2014; Di Rosa *et al.* 2016; Mazur *et al.* 2021; Pinteac *et al.* 2021). Excess levels of CLPs are associated with diseases that exhibit chronically inflamed tissues, such as cancer, asthma, and arthritis, and there they promote the disease process rather than mitigate it (Lee *et al.* 2011; Qureshi *et al.* 2011; Di Rosa *et al.* 2016; Kzhyshkowska *et al.* 2016; Mazur *et al.* 2021; Pinteac *et al.* 2021).

The enzymatically active members of the family 18 glycosyl hydrolases hydrolyze the glycosidic bonds of chitin, a polysaccharide present in plant, fungal, bacterial, and animal species (Samac *et al.* 1990; Fuhrman *et al.* 1992; Miyashita and Fujii 1993; Watanabe *et al.* 1993; Tharanathan and Kittur 2003). CLPs, on the other hand, lack hydrolytic activity due to substitution of a key amino acid (glutamic acid) in the protein's catalytic domain (e.g. with glutamine in *Drosophila* Idgfs and human CHI3L2, or with leucine in human CHI3L1; Kirkpatrick *et al.* 1995; Recklies *et al.* 2002; Varela *et al.* 2002). This mutation was facilitated by duplication of ancestral chitinases, followed by subsequent mutations and further duplications (Bussink *et al.* 2007). Over

evolutionary time, CLPs acquired new functions that do not require chitinase activity.

Extensive research in humans has identified four CLPs: chitinase 3 like 1 (CHI3L1), chitinase 3 like 2 (CHI3L2), oviductal glycoprotein 1 (OVGP1), and stabilin-interacting CLP (SI-CLP). Most studies have focused on the expression patterns of CLPs and their clinical relevance as potential biomarkers of disease or as targets for therapy (Mazur *et al.* 2021; Pinteac *et al.* 2021). Analyses of the associated molecular mechanisms are limited to a few studies identifying binding partners, receptors, or signaling pathways (Fusetti *et al.* 2003; Kzhyshkowska *et al.* 2004, 2006; Shao *et al.* 2009; Zhang *et al.* 2009; Francescone *et al.* 2011; Areshkov *et al.* 2012; He *et al.* 2013; Libreros *et al.* 2013; Low *et al.* 2015; Malik *et al.* 2015; Guan *et al.* 2020), but these studies relied on in vitro cell culture, binding assays, immunohistochemistry, or biochemical methods rather than whole-animal models. To understand the molecular mechanisms of CLP function in physiological and pathological contexts, we need to analyze function in vivo, preferably in a model organism that would allow definitive functional tests.

The 6 *Drosophila* Idgfs are encoded by genes located at four sites in the genome: *Idgf1*, *Idgf2*, and *Idgf3* are clustered together on the left arm of chromosome 2 (2L), *Idgf4* lies on the X chromosome, while *Idgf5* and *Idgf6* reside ~1.7 Mb apart on the right arm of chromosome 2 (2R; Fig. 1a and Supplementary Table 1; Kirkpatrick *et al.* 1995; Kawamura *et al.* 1999; Zurovcova and
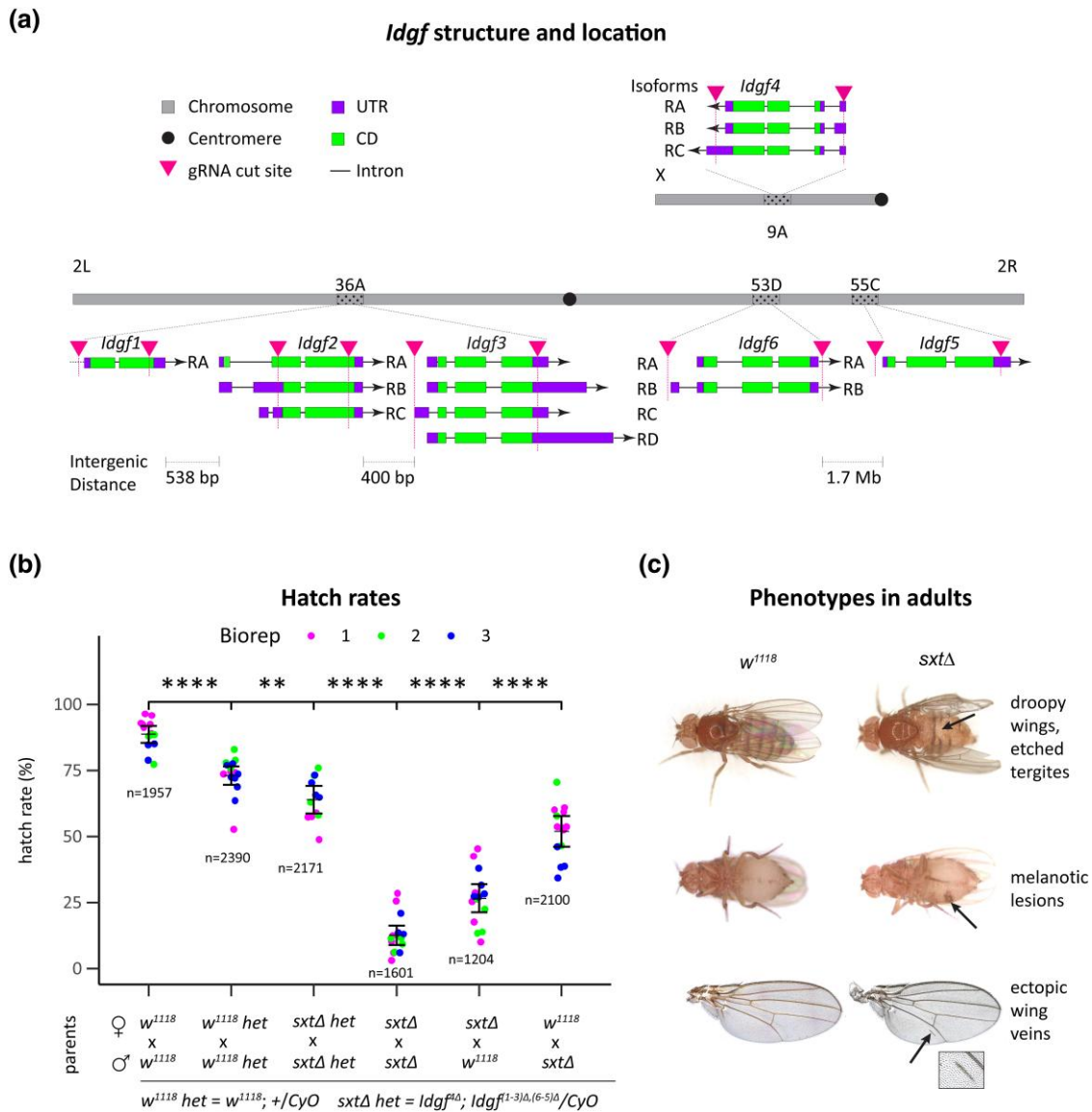
Fig. 1. *Idgf* complete knockouts are not entirely lethal. a) Diagram shows cytological locations of *Idgf* genes and structure of transcript isoforms, including 5′ and 3′ untranslated regions, coding sequences, and introns. Black arrows on transcripts indicate the orientation of transcription in the plus (right-pointing) or minus (left-pointing) direction. Arrowheads indicate approximate cut sites for deleting each *Idgf* gene. In the *sxtΔ* mutant, the deletion of *Idgf2* and *Idgf3* spans the entire sequence from the *Idgf2* 5′ upstream cut site to the *Idgf3* 3′ downstream cut site, deleting both genes and the 400 base pairs between them. b) Homozygous and heterozygous *sxtΔ* mutants have low hatch rates relative to control (w^{1118}). Dots represent egg-laying assays sampled from 3 independent biological replicates with 350–852 eggs analyzed per replicate. Error bars indicate 95% confidence intervals. Significance is based on pairwise *t*-tests with *P*-values adjusted for multiple comparisons (Benjamini–Hochberg). ** $P \leq 0.01$, **** $P \leq 0.0001$. c) Phenotypes exhibited by adult offspring of homozygous *sxtΔ* parents (i.e. F2 adults). Top row, dorsal view: 40% of males ($n = 48$) and 71% of females ($n = 31$) had etched tergites (arrow). Of the same flies, 60% of males and 48% of females exhibited abnormal wing postures: wings were held out and down ("droopy" wings) or held out and up. Middle row, ventral view: rarely (<5% of flies), *sxtΔ* mutants displayed dark cuticle patches (arrow) reminiscent of melanotic clots. Bottom row: 5% of male wings ($n = 78$ wings) and 74% of female wings ($n = 43$ wings) displayed ectopic wing veins (arrow). w^{1118} flies displayed none of these phenotypes ($n = 20$ males and 20 females). Anterior is up, distal is to the right.

Ayala 2002). Although now defined with a common nomenclature, the proteins were originally identified through different routes. Idgf6 (previously called DS47) was isolated from media from cultured Schneider line-2 (S2) cells, which have macrophage-like properties (Kirkpatrick *et al.* 1995). Idgf1, Idgf2, Idgf3, and Idgf4 were isolated from conditioned media from imaginal disk cell culture (Clone 8 cells; Kawamura *et al.* 1999). Idgf5 was identified by computer search of the *Drosophila* genome (Zurovcova and Ayala 2002).

Idgf proteins exhibit about 50% amino acid identity with each other and 15–25% amino acid sequence homology to family 18 glycosyl hydrolases, which include the chitinases (Kawamura *et al.*

1999; Varela *et al.* 2002). Consistent with their identification as secreted proteins, Idgfs and their human orthologs have an N-terminal signal sequence and an N-linked glycosylation sequence (Nyirkos and Golds 1990; Arias *et al.* 1994; Kirkpatrick *et al.* 1995; Hu *et al.* 1996; Renkema *et al.* 1998; Kawamura *et al.* 1999; Meng *et al.* 2010; Schimpl *et al.* 2012). The proteins form a characteristic barrel structure composed of 8 parallel beta sheets surrounded by 8 anti-parallel alpha helices (Varela *et al.* 2002).

Idgfs promote growth, proliferation, polarization, and motility in cultured cells (Kawamura *et al.* 1999). They participate in wound healing, protect against infection by nematodes (Kucerova *et al.* 2016; Broz *et al.* 2017), function in detoxification of cells
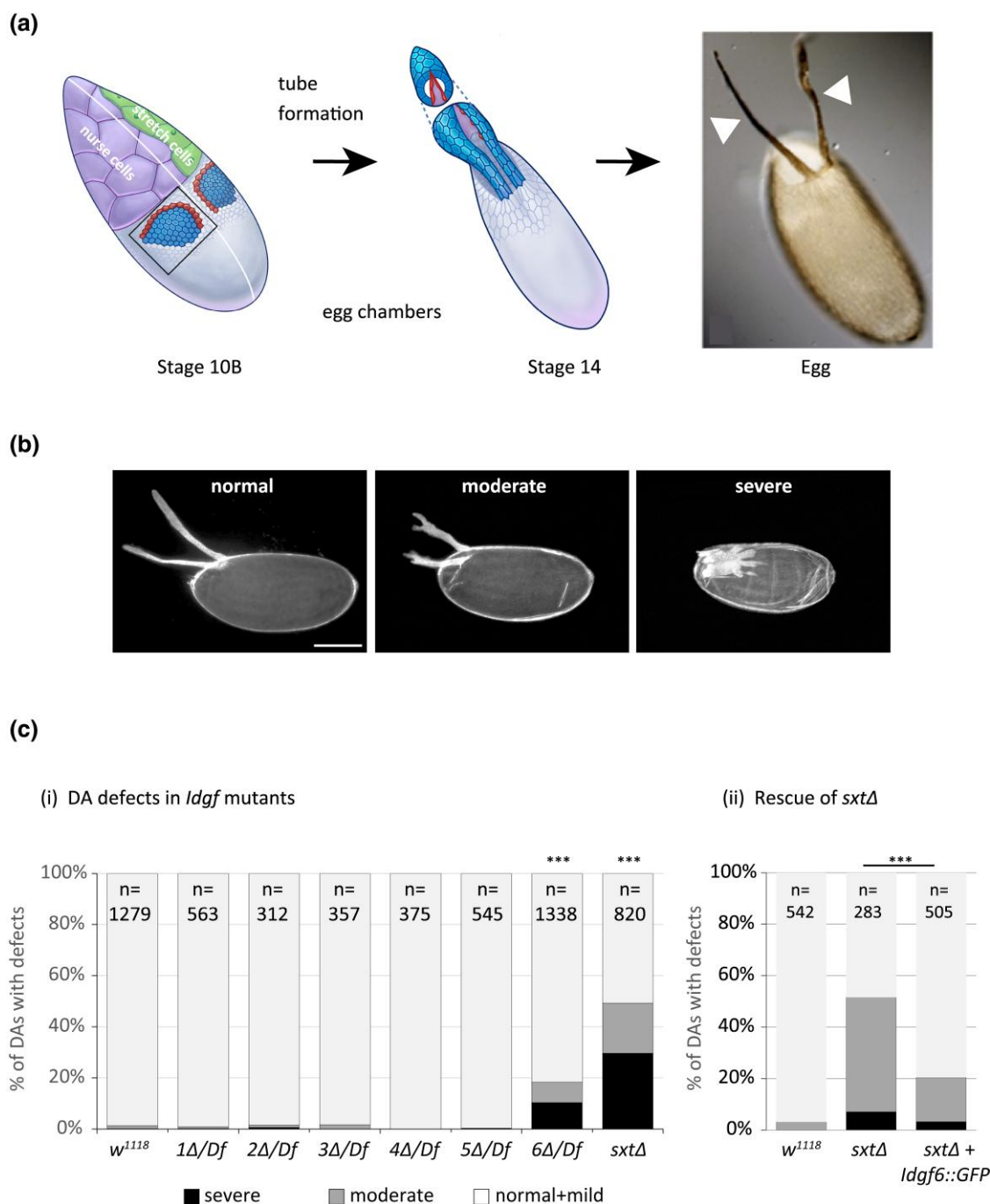
Fig. 2. *Idgf* mutants exhibit defects in DA tube formation. a) DA formation. Roof cells (blue) and floor cells (red) change shape and reorganize to make 2 DA tubes. Stretch cells, cut away to show nurse cells, guide tube elongation. DAs (arrowheads) of the laid egg bring air to the embryo that is developing inside the eggshell. b) Representative examples of DA morphology categorized into normal, moderate, and severe phenotypes. Scale bar = 100 μm. c) Moderate and severe DA phenotypes are significantly increased in eggs laid by *Idgf6Δ/Df* and *sxtΔ* females relative to the w^{1118} control, indicating defects in tubulogenesis during oogenesis. *Idgf1Δ/Df*, *Idgf2Δ/Df*, *Idgf3Δ/Df*, *Idgf4Δ/Df*, and *Idgf5Δ/Df* single mutants do not significantly affect DA morphology [C(i)]. Expression of a wild-type *Idgf6* transgene in *sxtΔ* mutant females partially rescues DA morphology [C(ii)]. Deficiency chromosomes specific to each mutant are listed in Supplementary Table 3. ***$P < 0.001$. Fisher's exact test, adjusted for multiple comparisons. Schematic diagrams in (a) are adapted with permission from Dorman *et al.* (2004).

(Broz *et al.* 2017), and participate in extracellular matrix organization required for molting (Pesch *et al.* 2016). To accomplish these functions, the Idgfs are not co-regulated, but rather, exhibit distinct expression patterns and respond to different stimuli. In the embryo, *Idgf* RNA is localized in cells adjacent to invaginating cells during tissue morphogenesis (Kawamura *et al.* 1999). In larvae and adults, Idgfs are expressed by hemocytes and the fat body

(functional equivalent of the liver) and secreted into the hemolymph (Kirkpatrick *et al.* 1995; Kawamura *et al.* 1999; Khush and Lemaitre 2000; Meister *et al.* 2000; Carton and Nappi 2001; Irving *et al.* 2001). Hemocytes and fat body both participate in innate immune responses. In the ovary, Idgfs are expressed in dynamic patterns specific to the different cell types of the egg chamber (Zimmerman *et al.* 2017). Both over- and under-expression in egg

chamber cells disrupt epithelial tube morphogenesis (Zimmerman *et al.* 2017; Espinoza and Berg 2020). Thus, Idgfs function in diverse processes in different tissues.

In this study, we focused on characterizing the physiological roles of the Idgfs by precisely deleting each of the *Idgf*s using the CRISPR/Cas9 system and assessing the effects of complete loss of function in various tissues and different life stages. We found that flies lacking all 6 Idgfs have low viability and fertility. Defects during germ cell formation or gonad formation in these mutants likely contribute to the observed low fertility. We detected numerous cuticle defects in adults, abnormal epithelial morphogenesis in egg chambers, and segmentation defects in embryos. Finally, we found that Idgfs regulate E-cadherin and cortical actin and protect epithelia against CO_2 exposure.

Materials and methods
Fly stocks

Bloomington stocks: w^{1118} (3605), *Df(2L)ED1102* (24113), *Df(1) ED6989* (9056), *Df(2R)BSC337* (24361), *Df(2R)Exel6064* (7546). VDRC stock: $Idgf6^{fTRG01331.sfGFP-TVPTBF}$ (Sarov *et al.* 2016). Stocks generated in this study and used in the experiments: $Idgf1^{\Delta}$, $Idgf2^{\Delta}$, $Idgf3^{\Delta}$, $Idgf4^{\Delta}$, $Idgf5^{\Delta}$, $Idgf6^{\Delta}$, $Idgf2^{-3\Delta}$, $Idgf^{(1\Delta, 2-3\Delta)}$, and $Idgf4^{\Delta}$; $Idgf^{(1\Delta, 2-3\Delta, 6\Delta, 5\Delta)}$ (sxtΔ). All *Idgf* mutants generated in this study, including all double and triple nulls, are listed in Supplementary Table 2. Flies were maintained on standard molasses food at 25°C.

Reagents and materials
Ovaries

- Dissecting dishes and forceps
- PBS, 10×, (combine NaCl 80 g, KCl 2 g, Na_2HPO_4 14.4 g, KH_2PO_4 2.4 g in 1 l of H_2O, pH to 7.4)
- PBT, 1% (vol/vol) or 0.1% Triton X-100 diluted in 1× PBS
- EBR, 10× (modified Ephrussi–Beadle Ringer's solution) 1.3 M NaCl, 47 mM KCl, 19 mM $CaCl_2$, and 100 mM HEPES pH to 6.9
- Paraformaldehyde, 4% (wt/vol), dilute 16% (wt/vol) EM-grade paraformaldehyde (Fisher Scientific, #50980487) in 1× PBS or PBT (defined above) at a ratio of 1:4
- Western blocking reagent (WBR; Sigma-Aldrich, #11921673001)

Embryos

- Flow Buddy–Benchtop flow regulator (Genesee, #59-122B)
- Nylon mesh (Elko Filtering Co., #03-110/47)
- Egg collection baskets: Falcon tube (15 or 50 ml) with the bottom cutoff and nylon mesh attached to bottom (e.g. melt the bottom edge slightly with a Bunsen burner and press on the nylon mesh)
- Double-sided sticky tape
- Whatman paper
- Pipette controller (e.g. Millipore Sigma, #BR25900)
- Pasteur pipettes, glass, 3.5 inches
- Petri dishes: Olympus 35 mm × 10 (Genesee Scientific, #32-103)
- Plastic fly bottles punched with holes (to make egg laying chambers when attached to apple juice plates)
- 30-Gauge syringe needles + plastic syringes
- PBTA (1× PBS, 1% BSA, 0.05% or 0.1% Triton X-100, 0.02% sodium azide)
- PBT [1× PBS with 0.1% (vol/vol) Triton X-100]

- Paraformaldehyde, 4% (wt/vol), dilute 16% (wt/vol) EM-grade paraformaldehyde (Fisher Scientific, #50980487) in 1× PBS or PBT at a ratio of 1:4
- 37% formaldehyde (e.g. Sigma-Aldrich, #252549)
- Apple juice plates, 175 ml H_2O, 25 ml 4× apple juice, 5 g of agar 1.2 g of methyl paraben. Heat in microwave until agar dissolves. Pour into Petri dish lids. Attach these plates to the plastic fly bottles using rubber bands.
- Bleach
- Heptane saturated with 37% formaldehyde: Combine equal volumes of heptane and 37% formaldehyde, shake the mixture vigorously for 15 s. Let the solution settle into the 2 phases. Prepare the solution the day before it is to be used, shaking the vial or bottle periodically throughout the day. The saturated heptane is the upper phase in the 1:1 heptane:formaldehyde stock. Store at room temperature (RT), protected from light, up to several months
- 1× embryo wash solution: 0.7% NaCl, 0.05% Triton X-100, H_2O
- Normal goat serum (NGS; Fisher Scientific, #10-000-C)
- Hoyer's mounting medium: Hoyer's stock is 30 g gum Arabic, 200 g chloral hydrate, 20 g glycerol, and 50 ml H_2O. Mounting medium is 4 parts Hoyer's stock:1 part H_2O:1 part lactic acid
- Vectashield mounting medium (Vector Laboratories, #H-2000-2)

Wings

- AquaPolymount mounting medium (Polysciences Inc, #18606-20)
- Ethanol

Generation of *Idgf* mutant fly lines

Deletions of the entire locus or most of the locus for each of *Idgf1*, *Idgf2*, *Idgf3*, *Idgf4*, *Idgf5*, and *Idgf6* were created using CRISPR/Cas9-catalyzed homology-directed repair. For each deletion, we designed and injected 3 vectors: 2 guide RNAs and 1 donor containing a Ds-Red eye reporter to aid in screening newly transformed flies. Using the FlyCRISPR algorithm (tools.flycrispr.molbio.wisc.edu/targetFinder), we designed guide RNAs targeting sites upstream and downstream of each gene. Guide RNAs were synthesized as 5′-phosphorylated oligos (Operon), annealed, and ligated into the BbsI sites of the pU6-BbsI-chiRNA plasmid (Addgene #45946). For the donor vector, we PCR-amplified ~1 kb homology arms from genomic DNA of the injection strain and cloned them into pHD-DsRed-attP (Addgene #51019). We co-injected guide RNA plasmids and donor vectors (Rainbow Transgenics) into *y vas-Cas9 w^{1118}* embryos (Bloomington 55821) and screened F1 flies for germline transmission of the DsRed reporter, followed by single-fly PCR and sequencing. The *Idgf* null strains were outcrossed to w^{1118}; +; + for 3 generations to remove background effects and remove the *vas-Cas9* transgene. All single *Idgf*-null lines are homozygous viable and fertile. See Supplementary Table 2 for information on strains carrying multiple null alleles.

Hatch rates, larval lethality, and pupal lethality

Eclosing male and female adults were collected over a few days, mated, and aged on apple juice plates with a dab of wet yeast paste for 2 days before egg collections. Eggs were counted and allowed to develop for >24 h at 25°C to allow hatching. Subsequently, unhatched eggs were counted to determine the hatch rates. Larval lethality was assessed by allowing adults to
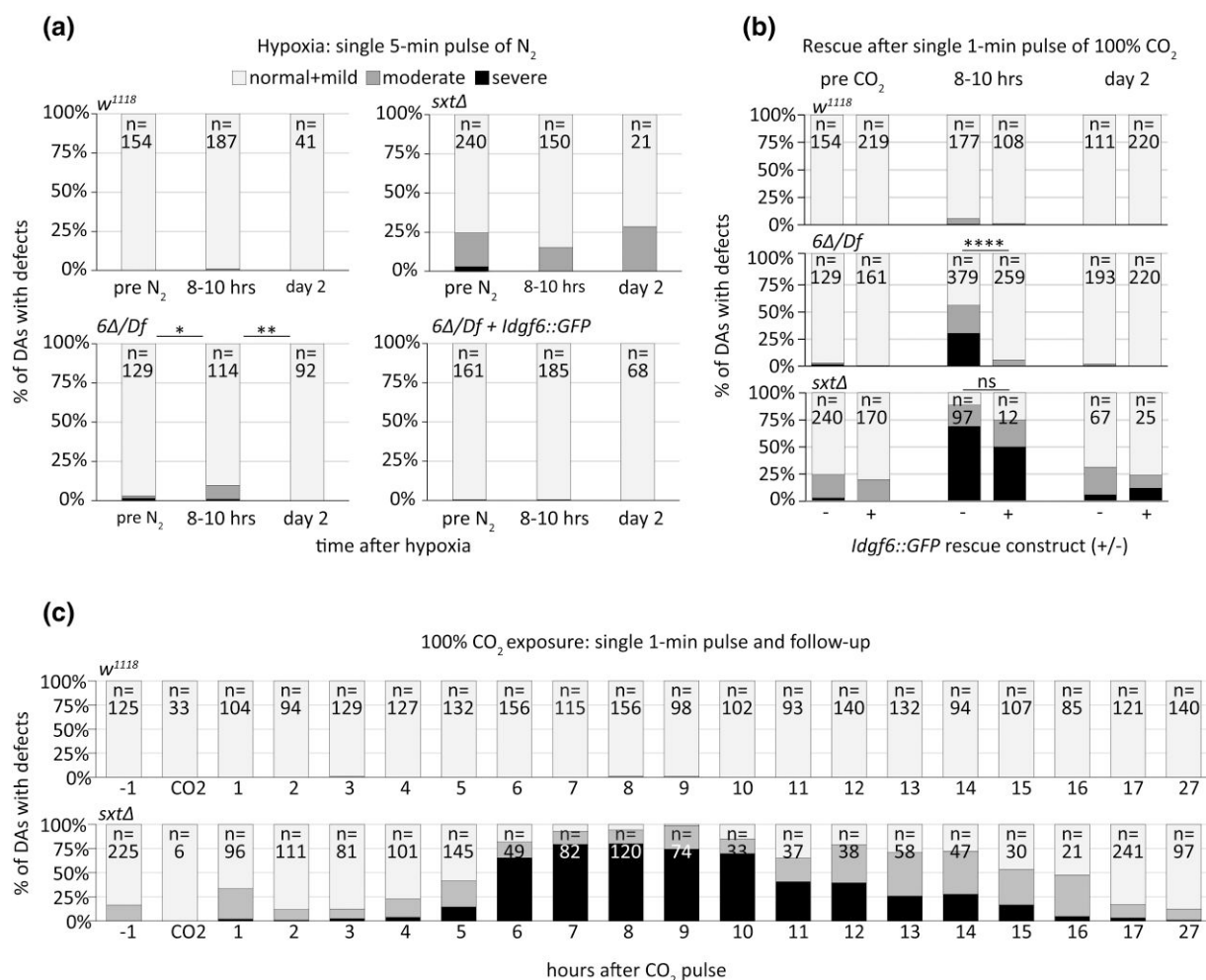
Fig. 3. Idgfs protect against CO_2 exposure. a) Effect of hypoxia on DA phenotype. Air is replaced with 100% N_2 for 5 min to induce hypoxia. DA phenotype is not significantly affected by hypoxia. b) Expressing a single copy of a wild-type *Idgf6* transgene rescues the DA *Idgf6Δ* phenotype induced by a single, 1-min pulse of 100% CO_2. The *sxtΔ* phenotype is partially but not significantly rescued ($P = 0.23$, Fisher's exact test). Proportions of defects peak at 8–10 h after the CO_2 pulse. The *Idgf6Δ* deletion is transheterozygous with a deficiency chromosome to cover potential background mutations. ****significance ($P \le 0.0001$, Fisher's exact test), NS = not significant. c) Hourly assessment of DA phenotype following a 1-min pulse of 100% CO_2. DA defects in eggs laid by *sxtΔ* females peak at 7–10 h after CO_2 exposure.

lay on apple juice plates and allowing the eggs to hatch. All living and dead 1st instar larvae were counted, and the live larvae were transferred to vials with standard fly food. The number of subsequent pupae represents the number of transferred larvae that survived larval development. Larval lethality was calculated by subtracting the number of pupae from the total number of larvae (live transferred + dead on plates). Pupal lethality was calculated by counting the number of empty pupal cases vs the number of dead pupae on the side of the vial. Care was taken to keep the food sufficiently hydrated to encourage pupariation on the sides of the vials rather than in the food.

Fertility assay

Virgins and males were collected over 2 days and aged for 2 days in vials with dry yeast. Equal numbers of males and females of the appropriate genotypes were crossed in embryo collection bottles on apple juice plates with a dab of wet yeast paste. After a 12-h pre-collection, embryos were collected for 4 h and aged for 1.5–2 h, after which they were washed off the plate, using embryo wash and water, into a collection basket made by sealing nylon mesh to a cutoff 50-ml Falcon tube. The basket was placed into a 100 × 50 Kimax low top beaker. Freshly prepared 50% bleach

was added and swirled for 90 s while viewing dechorionation under a dissecting microscope. The basket was removed from the bleach and rinsed thoroughly with embryo wash and ddH₂O. The embryos were rinsed into a 35-mm Petri dish with embryo wash and examined on an inverted phase contrast microscope. Embryos that were visibly developing (Wieschaus and Nüsslein-Volhard 1986) were scored as fertilized. The percentage of fertilized embryos was calculated from averaging counts from 2 collections each from 2 biological replicates.

Tissue processing and immunohistochemistry
Ovaries

For CO_2 experiments in Figs. 4 and 5, adult females were exposed to a 1-min pulse of 100% CO_2 by inserting the CO_2 needle into a glass vial. Thirty minutes after CO_2 exposure, the flies were killed by placing them in 100% ethanol. Ovaries were dissected in EBR, fixed for 20 min in 4% (wt/vol) paraformaldehyde, permeabilized for 1 h in PBS with 1% Triton X-100, and blocked for 1 h in WBR. Ovaries were washed in PBT, incubated on a nutator O/N at 4°C in PBT with mouse anti-Broad (DSHB 25E9.D7, 1:500), rat anti-E-cadherin (DSHB DCAD2-c, 1:50) and 5% NGS, washed in PBT, incubated for 1 h at RT in Alexa Fluor goat anti-mouse
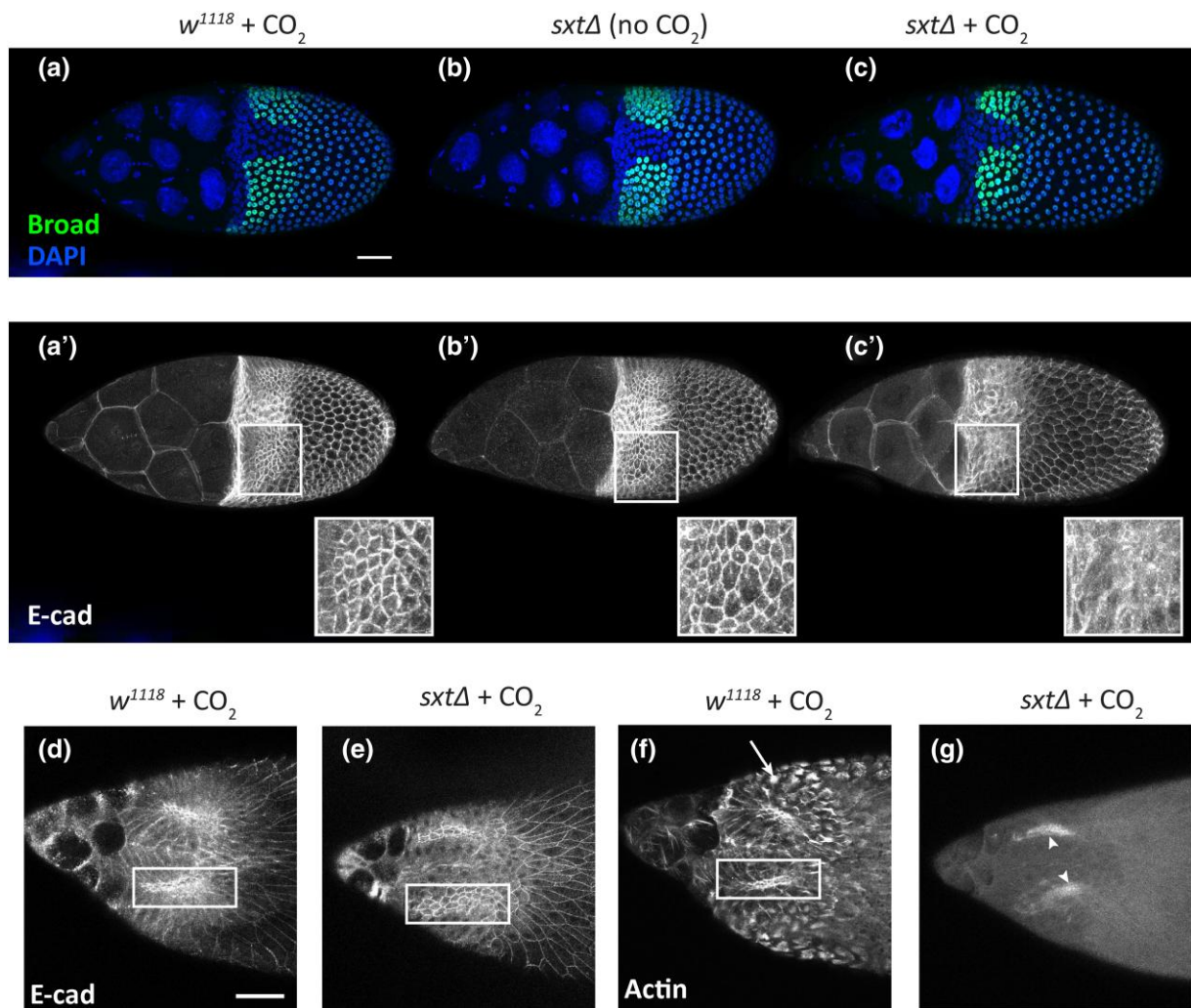
Fig. 4. *sxtΔ* mutants exhibit defects in cell morphology but not patterning of DA-forming cells. Images are projections of Z-stacks. a–c') Stage 10B egg chambers. Top row (a–c): High expression of Broad marks the roof cells in the DA primordium, DAPI indicates the nuclei. Patterning is normal in *sxtΔ* mutant exposed to CO_2. Lower row (a'–c'): E-cadherin delineates the apico-lateral cell junctions in follicle cells. Epithelial morphology and E-cadherin localization are disrupted in *sxtΔ* mutant DA-forming patches after a single pulse of 100% CO_2 exposure. Insets show magnified views outlined by the white rectangles. d–g) Stage 12 egg chambers. Filamentous actin is visualized with rhodamine-phalloidin. DA roof cells (white rectangles) form a wider appendage and are less constricted in the *sxtΔ* mutant (e) compared with control (*w^{1118}*) (d) egg chambers. f) As shown in *w^{1118}* egg chambers, basal cell membranes normally exhibit bright spots of actin localization (arrow). g) In *sxtΔ* mutants, filamentous actin is reduced in cell membranes after CO_2 exposure. Arrowheads in the *sxtΔ* + CO_2 image indicate chorion autofluorescence. Images are representative of 68 egg chambers: *w^{1118}* no CO_2 (not shown) (n = 7 Stage 10B and 6 Stage 12 egg chambers), *w^{1118}* plus CO_2 (n = 11 Stage 10B and 9 Stage 12), *sxtΔ* no CO_2 (n = 10 Stage 10B and 7 Stage 12), *sxtΔ* plus CO_2 (n = 10 Stage 10B and 12 Stage 12). Scale bars = 50 μm.

(Invitrogen A-11001, 1:200), goat anti-rat (Invitrogen A-21247, 1:200), rhodamine phalloidin (Abcam ab235138, 1:500), and DAPI (1 μg/ml), washed in PBT, mounted on slides, and imaged on a Leica SP8X LSM.

Embryos requiring manual devitellinization and phalloidin staining

Females were aged for 2 days with wet yeast paste. Males and females were mated and allowed to lay on apple juice plates O/N or for a few hours to obtain a range of desired stages. All aspects of this experiment prior to dechorionization were done at 25°C. For CO_2 experiments only, embryos were exposed to 100% CO_2 for 2 min (Stages 8–11) or 6 min (Stages 3–5) by inserting the CO_2 needle through a hole in the plastic fly bottle. The CO_2 was humidified by flowing the gas through a bubbler while the flow rate was held precisely at 3.5 L per minute using the Flow Buddy. Using a paint brush and embryo wash, embryos were washed from plates into

a basket and rinsed with embryo wash using a squirt bottle, then dechorionated in 50% bleach (1:1 bleach:H_2O) for 2 min by submerging the mesh end of the basket in a Falcon tube with the bleach. The dechorionated embryos were rinsed with embryo wash in the basket, then transferred to a 1.5 ml Eppendorf tube by squirting embryo wash onto the outside end of the mesh and into the Eppendorf tube. For hand devitellinization, embryos were fixed for 40 min in 1 ml of heptane saturated with 37% formaldehyde. Using a pipette tip with the tip cutoff and pre-treated in PBTA, embryos were transferred to Whatman paper for ~30 s to allow the heptane to evaporate. The Whatman paper was placed embryo side down on the tape, gently tapped until embryos were stuck to the tape, and the embryos were immediately covered with PBS. Vitelline membranes were manually removed using 30-Gauge syringe needles. Using a pipette controller attached to a glass Pasteur pipette pre-treated with PBTA, embryos were transferred to PBTA (PBS with 0.1% Triton X-100, 1% BSA and
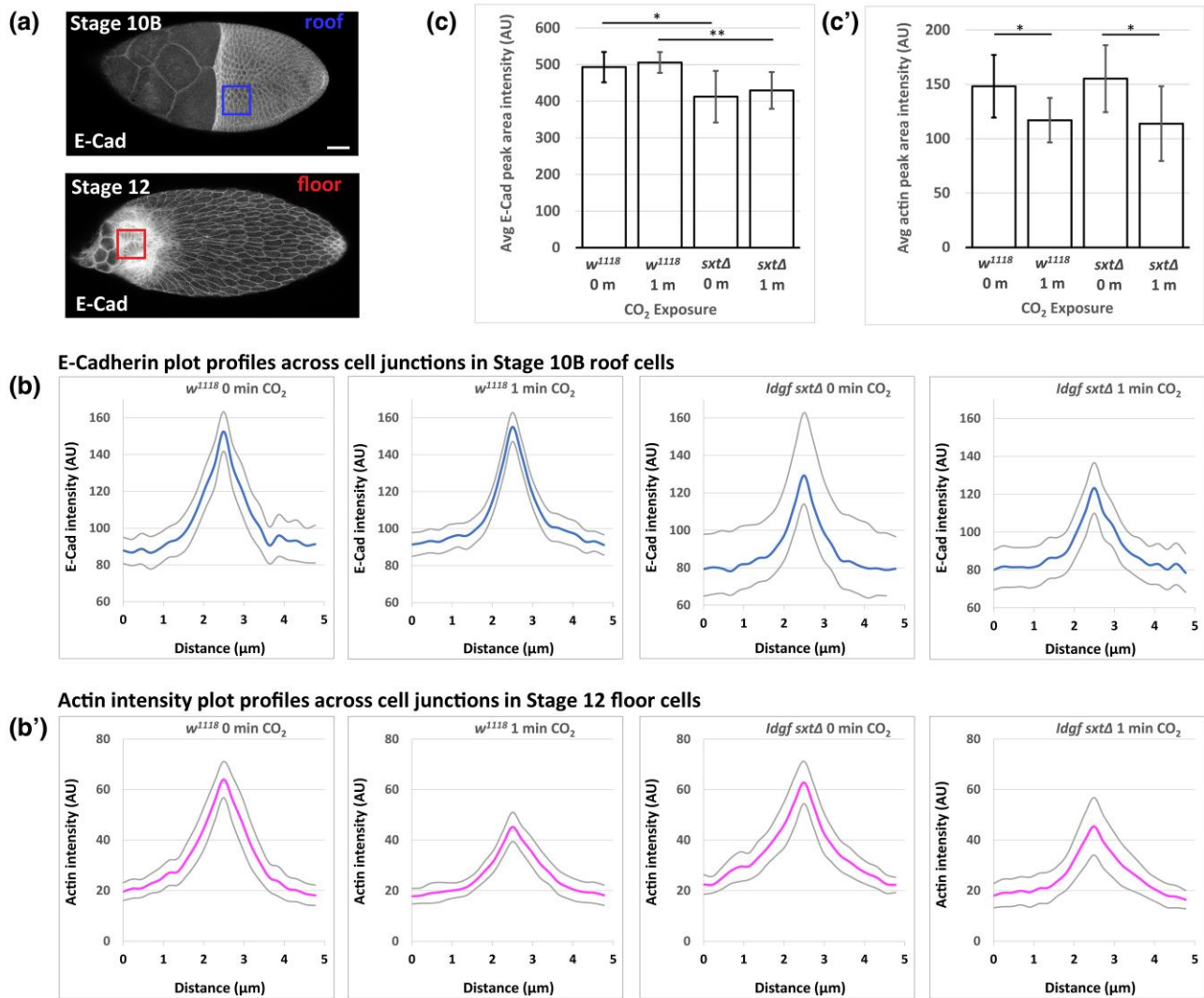
Fig. 5. Cortical actin and E-cadherin respond differently to CO_2 in *sxtΔ* egg chambers. a) Fluorescent intensity in Stage 10B roof cells (square) and Stage 12 floor cells (square). Measurements were made apically in w^{1118} and *sxtΔ* egg chambers in both E-cadherin and actin channels. Shown are examples of E-cadherin in w^{1118} egg chambers. Scale bar = 50 µm. b) Comparison of w^{1118} and *sxtΔ* fluorescence intensity plot profiles averaged across 3 cell membranes, from the center of 1 cell to the center of the neighboring cell, averaged over at least 6 egg chambers for each genotype and each exposure regime as indicated. Plots show mean (inner thicker plot line) and 95% confidence limits (outer thinner plot lines). c) Integrated area under the curves in (b) and (b') averaged over all measurements. Error bars show 95% confidence limits. $^*P \le 0.05$, Student's *t*-test, Benjamini–Hochberg adjusted *P*-values.

0.02% sodium azide) for staining or to PBTA (with 0.05% Triton X-100) for storage at 4°C. Stage 3–5 embryos were incubated with DAPI (1 µg/ml), and rhodamine phalloidin (Abcam ab235138, 1:500) for 1 h, and washed in PBTA (with 0.05% Triton X-100) for 1 h, rinsed 3× in PBS, and mounted in Vectashield mounting medium. Stage 8–12 embryos were incubated with rat anti-E-cadherin (DSHB DCAD2, 1:50) and mouse anti-Engrailed (DSHB 4D9) concentrate (1:20) or supernatant (1:50) in PBTA (with 0.1% Triton X-100) and 5% NGS O/N at 4°C, washed 2× 30 min in PBTA (with 0.1% Triton X-100), incubated for 1 h at RT in PBTA with 0.1% Triton X-100, 5% NGS, DAPI (1 µg/ml), rhodamine phalloidin (1:500), Alexa Fluor goat anti-mouse 488 and anti-rat 647, washed 2× 30 min in PBTA with 0.1% Triton X-100, rinsed 3× (quick rinses) in PBS, and mounted on slides with Vectashield mounting medium.

Embryos not requiring phalloidin staining
Embryos in Supplementary Figs. 3, d, d′, e, and e′ and 4, a and a′) were dechorionated and fixed in 1:1 heptane:4%

paraformaldehyde for 20 min. The paraformaldehyde layer was removed and replaced with an equal amount of 100% methanol and shaken vigorously for 30 s to remove the vitelline membranes. All liquid was removed, and embryos were rinsed with methanol. Embryos were rehydrated by removing ~1/4 of the methanol and replacing it with PBT. This rehydration process was repeated 2×, and then the embryos were rinsed 3× in PBT. Embryos were incubated in PBT with 5% NGS, rabbit anti-Vasa (Paul Lasko, 1:2,000) and mouse anti-Engrailed (DSHB 4D9, 1:50) O/N at 4°C on a nutator. Primary antibody solution was removed and embryos were washed 3× with PBT over an hour. Secondary antibody incubation was performed at RT for 1 h with Alexa Fluor (Invitrogen) goat anti-mouse (1:200) and goat anti-rabbit (1:200) in PBT and 5% NGS.

Embryos expressing Idgf6-GFP in Supplementary Fig. 3, f and g were dechorionated and rinsed 3× in PBS. PBS was removed and 1 ml of heptane saturated with 37% formaldehyde was added. The tube was shaken vigorously for 15 s and allowed to stand for 5 min at RT. To devitellinize the embryos, the saturated

heptane was removed and replaced with 0.5 ml of methanol and 0.5 ml of heptane. The tube was shaken vigorously for 15 s and allowed to stand for 1 min. After devitellinization, the heptane and methanol were removed, along with the embryos that did not sink, but leaving the embryos that did sink at the bottom of the tube. One milliliter of methanol was added and embryos were rehydrated by performing 5-min washes in the following series of methanol:PBS solutions: 80%:20%, 60%:40%, and 20%:80% followed by washing for 30 min in PBS. PBS was removed and embryos were incubated on a nutator O/N at 4°C in PBTA (with 0.1% Triton X-100), rat anti-Vasa (DSHB anti-vasa-c, 1:500), and 5% NGS. The antibody solution was removed, and the embryos were rinsed 3× in PBTA (with 0.05% Triton X-100) and washed for 30 min in PBTA (with 0.05% Triton X-100), rinsed 3× in PBTA (with 0.05% Triton X-100), and incubated on a nutator for 2 h at RT in PBTA (with 0.1% Triton X-100), 5% NGS, and Alexa Fluor (Invitrogen) goat anti-rat (1:400). Antibody solution was removed, embryos were rinsed 3× in PBTA (with 0.05% Triton X-100) and washed for 30 min in PBTA (with 0.05% Triton X-100), rinsed 3× in PBS, mounted on slides in AquaPolymount, and imaged on a Leica SP8X LSM.

Wing area measurements

Wings were dissected in either PBS or 70% EtOH, transferred to 100% EtOH, and mounted in AquaPolymount. For wing measurements, images were acquired on a Nikon Microphot-FX microscope equipped with an AmScope MU1203-FL digital camera. Wing blade areas were measured using the segmented line tool in the ImageJ software (Version 1.53q) to outline the wing blade. The area within the outline was calculated in ImageJ using Analyze > measure. High resolution wing images in Fig. 1 were acquired on a Leica Inverted Multidimensional Widefield microscope.

Embryo/larval cuticle preps

Embryos and 1st instar larvae were washed from apple juice egg collection plates with embryo wash into egg collection baskets and dechorionated (2–3 min in 50% bleach). Embryos were rinsed and transferred to 1.5 ml Eppendorf tubes. Embryos were devitellinized by adding 1:1 heptane:methanol and shaking vigorously for several minutes or by vortexing. The heptane and undevitellinized embryos floating at the interphase were removed and the devitellinized embryos were rinsed 3 times in methanol. Embryos were mounted in Hoyer's mounting medium and baked overnight at 60°C to dissolve internal tissue. The embryos and larvae were imaged on a Leica Inverted Multidimensional Widefield microscope.

Dorsal appendage phenotype analysis

Eclosing adults were collected for a few days and aged for 2 days on apple juice plates with wet yeast paste. Plates were changed daily. Flies were exposed to either 100% CO_2 or 100% N_2 by inserting the CO_2 (N_2) needle through a hole in the plastic bottle for 1-min (CO_2) or 5-min (N_2). The CO_2 was humidified by flowing the gas through a bubbler. For the 20% CO_2, flies were continuously exposed to CO_2 in a regulated CO_2 chamber for 1.5–2 days or 7–8 days. Timing of egg collection after gas exposure was according to the regimes indicated in Fig. 3 and Supplementary Fig. 5. Eggs were rinsed into a mesh basket with embryo wash, then transferred to an Eppendorf tube. Eggs were mounted in Hoyer's medium and baked O/N at 60°C. The slides were imaged on a Nikon Labophot-2 microscope equipped with an AmScope MU1203-FL digital camera. Dorsal appendages (DAs) were scored blind and

categorized phenotypically as normal/mild, moderate, or severe. Fisher's exact test was used for the statistical analysis.

Image analysis and quantification

For actin and E-cadherin intensity measurements in egg chambers, images were acquired as 8-bit images at the same laser intensities and detector settings on a Leica SP8X LSM. Using ImageJ, we measured E-cadherin and actin intensity across the cell membrane in 3 pairs of cells, from the center of 1 cell to the center of the neighboring cell, in at least 6 egg chambers for each genotype and compared egg chambers exposed to CO_2 to egg chambers not exposed to CO_2. Plot profiles across 5.0 μm were averaged over all egg chambers for each genotype and treatment. Total E-cadherin or actin was calculated by integrating the area under the mean-plot-profile curve using the trapezoidal rule. Data analyses were performed in Excel. Statistical analyses were performed in Excel and R.

For actin and E-cadherin intensity measurements in embryos, images of both genotypes and treatments were acquired as 16-bit images at the same laser intensities and detector settings on a Leica SP8X LSM. For each individual channel and optical plane being measured, background was subtracted, and a median filter was applied (rolling ball radius of 2.0) prior to measurements. For each genotype, we measured E-cadherin and actin fluorescent intensity as above, across the cell membrane in 6 pairs of cells per embryo, with $n = 10$ embryos for each treatment (no CO_2, +CO_2) within 3 bioreplicates, except for $sxt\Delta$ bioreplicate 3, no CO_2 ($n = 6$ embryos). Plot profiles across 3.5 μm were averaged over all embryos for each genotype and treatment. Total E-cadherin or actin was calculated by integrating the area under the mean plot profile curve using the trapezoidal rule. Data analyses were performed in Excel. Statistical analyses were performed in Excel and R.

Statistical analysis

All statistical analyses were performed in either Excel (Version 2209) or R (Version 4.0.2). Comparisons of categorical data (i.e. curly vs straight wing phenotypes and DA phenotypes) were performed in R using Fisher's exact test. t-tests were performed in Excel, and adjustments for multiple comparisons were performed in R using the Benjamini–Hochberg method.

Results
Idgf null lines

To begin to understand how Idgfs function, we developed Idgf null lines using the CRISPR/Cas9 system. We deleted the coding region and all or part of the untranslated regions of each Idgf, creating single, double, triple, and more mutant lines, as well as a line with all 6 deletions (w^{1118} $Idgf4\Delta$; $Idgf^{(1\Delta, 2-3\Delta, 6\Delta, 5\Delta)}$, termed "sextuple mutant" and designated as $sxt\Delta$; Fig. 1a, Supplementary Fig. 1, and Table 2). Since Idgf1 and Idgf6 reside in introns of CG5888 and N-Acetylgalactosaminyltransferase 9 (Pgant9), respectively, we designed the deletions in such a way as to minimize the impact on non-coding regions and leave all exons intact in CG5888 and Pgant9. Similarly, the Idgf2 deletion was a partial deletion to avoid removing any part of CG5888, which has a transcriptional start site in the first intron of Idgf2 (see FlyBase for detailed information about each Idgf locus). We confirmed the extent and structure of each deletion by sequence analyses (See Supplementary Data File 16 for sequence definitions, FASTA sequences uploaded to NCBI, GenBank accession numbers OP745290–OP745323). In the laboratory environment of rich food and benign growth

conditions, we found no highly penetrant defects in any single mutant. *sxtΔ* flies, however, exhibited numerous phenotypes described below.

sxtΔ mutants have low viability and fertility

Viability and fertility depend on many developmental processes that require patterning, growth, and cell migration. We assessed the function of Idgfs in this context by quantifying hatch rates for offspring from *sxtΔ* homozygous flies and from *sxtΔ* flies carrying the second chromosome CyO balancer (w^{1118} *Idgf^{4Δ}*; *Idgf$^{(1Δ,\ 2–3Δ,\ 6Δ,\ 5Δ)}$*/CyO). We compared these rates to hatch rates of offspring from w^{1118} and w^{1118} carrying the same second-chromosome balancer (w^{1118}; +/CyO) (Fig. 1b). See Supplementary Data File 1 for supporting data.

The expected proportions of genotypes for offspring from w^{1118}; +/CyO parents is 25% homozygous w^{1118}; +/+, 50% w^{1118}; +/CyO, and 25% homozygous w^{1118}; CyO/CyO. Lethality for CyO/CyO offspring occurs in late embryonic or early larval development (Kidwell 1972). For offspring of this w^{1118}; +/CyO background, we observed a hatch rate of 73% compared with a hatch rate of 64% in offspring from w^{1118} *Idgf^{4Δ}*; *Idgf$^{(1Δ,\ 2–3Δ,\ 6Δ,\ 5Δ)}$*/CyO parents. The lower hatch rate for embryos derived from the *sxtΔ*/CyO background indicates that reduction of Idgfs moderately impacts embryonic development and/or the fertility of the male parents (i.e. more of the laid eggs were not fertilized). For the heterozygous offspring from this cross (embryos carrying the CyO chromosome), maternal and zygotic contributions of wild-type Idgfs come only from the CyO chromosome. In the *sxtΔ* homozygous embryos, all zygotic expression of Idgfs is lost. Consistent with maternal loading of *Idgf* transcripts (Zimmerman *et al.* 2017), maternal and zygotic loss of Idgfs is more detrimental: nearly 90% of eggs laid by *sxtΔ* females mated to *sxtΔ* males fail to hatch. In comparison, only about 12% of eggs laid by w^{1118} parents fail to hatch. Surprisingly, some *sxtΔ* escapers survive to adulthood, and when crossed to w^{1118} flies, these escapers are weakly fertile (Fig. 1b).

Heterozygous offspring from *sxtΔ* females crossed to w^{1118} males have a higher hatch rate (26.5%) than embryos from a cross between *sxtΔ* homozygotes, presumably due to zygotic expression of wild-type Idgfs, and embryos from w^{1118} females crossed to *sxtΔ* males, which have both maternal and zygotic *Idgf* expression in embryos, have a 52% hatch rate (Fig. 1b and Supplementary Data File 1). This percentage is lower than the hatch rate from the *Idgf^{4Δ}*; *Idgf$^{(1Δ,\ 2–3Δ,\ 6Δ,\ 5Δ)}$*/CyO cross, possibly reflecting greater fertility of the males carrying the CyO balancer, which expresses wild-type Idgfs. These results indicate that maternal and zygotic expressions of wild-type Idgfs contribute to embryonic development and adult fertility.

To determine what portion of laid eggs were either unfertilized or had arrested before any noticeable development had taken place, we examined embryos from crosses between homozygous w^{1118} males and females, between *sxtΔ* males and females, between w^{1118} females and *sxtΔ* males, and between *sxtΔ* females and w^{1118} males (Supplementary Data File 15). Embryos were collected for 4 h and aged for 1.5–2 h, after which they were dechorionated, placed in a petri dish containing embryo wash, and examined on an inverted phase contrast microscope. 12% of all embryos resulting from the $w^{1118} \times w^{1118}$ cross were undeveloped, implying that the ~12% of w^{1118} embryos that fail to hatch (see above) are unfertilized or undeveloped. 37% of embryos from the *sxtΔ* × *sxtΔ* cross are unfertilized or undeveloped. This observation suggests that out of the remaining laid eggs, 13% hatch and 50% die as embryos (see above). 31% of embryos from *sxtΔ* males crossed to w^{1118} females were undeveloped, indicating lower

fertility in *sxtΔ* males compared with w^{1118} males. *sxtΔ* females also were less fertile: 31% of embryos from w^{1118} males crossed to *sxtΔ* females were undeveloped. This result could indicate a deleterious effect on very early development due to the lack of maternally contributed Idgfs; alternatively, *sxtΔ* females have a greater propensity to lay unfertilized eggs. Thus, embryonic lethality is higher in embryos resulting from crosses between *sxtΔ* × *sxtΔ* flies, w^{1118} females × *sxtΔ* males, or *sxtΔ* females × w^{1118} males.

In addition to losses due to undeveloped embryos or losses during embryonic stages, lethality occurred during larval development. 39% of control larvae (offspring of w^{1118} parents carrying the CyO chromosome) died during larval development compared with 62% of *sxtΔ* larvae (offspring of parents carrying the CyO chromosome). CyO/CyO individuals die during late embryonic development or as 1st instar larvae (Kidwell 1972), so a portion of the larval lethality could have resulted from hatched CyO/CyO individuals. Larvae might also have succumbed due to handling when transferring animals from egg-laying plates to vials. Pupal lethality was 7% in both control and *sxtΔ* pupae. See Supplementary Data File 2 for supporting data.

To further explore the effect of loss of Idgfs on viability and development, we compared eclosion rates between homozygous (straight-winged) and heterozygous (curly winged) adult offspring of heterozygous parents (w^{1118}; +/CyO or w^{1118} *Idgf^{4Δ}*; *Idgf$^{(1\ Δ,\ 2–3Δ,\ 6Δ,\ 5Δ)}$*/CyO males and females). Considering the lethality of homozygous CyO/CyO flies, the expected Mendelian fractions of curly vs straight-winged adults should be 2/3 heterozygous (curly winged) and 1/3 homozygous (straight-winged) flies. Fisher's exact test demonstrated that the relative fractions of wing phenotypes in the *sxtΔ* background (73% curly, 27% straight) deviates significantly from the relative fractions of wing phenotypes in the w^{1118} background (69% curly, 31% straight; $P = 0.0091$; Supplementary Fig. 2a and Data File 3). Furthermore, *sxtΔ* homozygotes are developmentally delayed compared with w^{1118} homozygotes. The fraction of *sxtΔ* homozygotes eclosing each day relative to the total after 3 days lagged behind the w^{1118} homozygotes (Supplementary Fig. 2b).

In summary, these results indicate that loss of all 6 Idgfs leads to lower fertility, lower hatch rates, greater embryonic and larval lethality, and delays in the timing of embryonic, larval, and/or pupal development.

sxtΔ mutants lay fewer eggs, have smaller ovaries, and fewer germ cells

In addition to lower hatch rates, *sxtΔ* females also laid fewer eggs, averaging 5.4 eggs per female per day, compared with 14.3 eggs per female per day for control females ($P = 0.018$, Student's *t*-test, 20 females, two 24-h collections; Supplementary Fig. 3b and Data File 4). Consistent with producing fewer eggs, *sxtΔ* females of the same age and treated to the same nutrient-rich diet had smaller ovaries relative to w^{1118} females. *sxtΔ* ovaries weighed about half as much (0.41 mg/ovary) as control ovaries (0.79 mg/ovary; $n = 24$ w^{1118} ovaries and 22 *sxtΔ* ovaries; Supplementary Fig. 3, a and a′).

Small ovaries could result from gonads with fewer germ cells. Germ cells form at the posterior pole of the embryo and migrate through the gut, guided by attractive and repellent cues, to the somatic gonadal precursors; together these 2 cell types form the gonads (Starz-Gaiano *et al.* 2001; LeBlanc and Lehmann 2017). To assess whether small ovaries and low fertility were consequences of defects in gonad formation, we marked germ cells with anti-Vasa antibody in control (w^{1118}) and *sxtΔ* embryos

(Supplementary Fig. 3, d, d', e, and e'). In the mutants, average germ-cell numbers in 3-h old blastoderm embryos were significantly reduced relative to embryos from control flies (Supplementary Fig. 3c and Data File 5, $P = 0.0016$, Mann–Whitney U test, $n = 12$ w^{1118} and 10 $sxt\Delta$ embryos). 16-h $sxt\Delta$ embryos had smaller gonads and exhibited germ cells outside of the gonads (Supplementary Fig. 3, e and e', $n = 8$ w^{1118} and 6 $sxt\Delta$ embryos). These defects potentially result from increased cell death or altered guidance cues, cell adhesion, or polarization. In support of the hypothesis that Idgfs facilitate population of germ cells into the gonads, we have observed a close association of Idgf6-GFP transgene expression with germ cells during embryonic Stages 4–7 (Supplementary Fig. 3, f and g, $n = 5$ Stage 4–7 embryos and $n = 5$ Stage 7–10 embryos).

Sextuple-mutant embryos lacking maternal and zygotic Idgfs exhibit segmentation defects

The insect body is organized in a series of segments, regulated by segmentation genes consisting of gap, pair rule, and segment polarity genes. For example, engrailed is a segment polarity gene that is expressed in the posterior 2 rows of each segment (Supplementary Fig. 4a) and participates in the development of denticle belts (DiNardo et al. 1985). Denticles are hook-like cuticle structures on the ventral side of each larval segment that provide traction for crawling (Supplementary Fig. 4b). During late embryogenesis, the larval epithelial cells that secrete the ventral cuticle have 1 of 2 fates: either they remain smooth, or they produce polarized, actin-based protrusions that form the denticles (Dilks and DiNardo 2010; Supplementary Fig. 4c). Maintenance of the segmental pattern of alternating smooth and denticle-producing stripes is regulated by the interactions between Wingless (Wg)-expressing cells and Engrailed (En)/Hedgehog (Hh)-expressing cells (Bejsovec and Martinez Arias 1991; Dougan and DiNardo 1992).

The pattern of En expression was disrupted in $sxt\Delta$ mutant embryos, both on a tissue level and within each cell (Supplementary Fig. 4, a' and d', $n = 12$ w^{1118} and 10 $sxt\Delta$ embryos). Smooth cuticle overlapped denticle belts, parts of neighboring belts sometimes fused together, and single rows of denticles localized within bands of smooth cuticle (Supplementary Fig. 4, b' and c'). 64% of $sxt\Delta$ embryos had disorganized denticle belts ($n = 14$ embryos) and 0% of w^{1118} ($n = 25$ embryos) exhibited defects. En aberrantly localized to cell membranes (Supplementary Fig. 4, d and d', and Data File 6) in 80% of $sxt\Delta$ embryos ($n = 10$) compared with 0% of w^{1118} embryos ($n = 12$).

We explored the defects in larval cuticle by examining the segmental pattern of denticle-producing and non-denticle-producing cell shapes in late-stage embryos and discovered an array of altered cell shapes and sizes (Supplementary Fig. 4, c and c', and Data File 7, $n = 0/9$ w^{1118} and $n = 11/14$ $sxt\Delta$ embryos with defects). This phenotype could be due to patterning defects, or, alternatively, the cells may have achieved proper cell fate but could not maintain proper positioning within a segment due to loss of cell-junction integrity. Cell polarity might also have been affected.

Adult flies display a variety of cuticle defects and lesions

Adult F1 and F2 $sxt\Delta$ flies exhibited several visible phenotypes (Fig. 1c). We quantified these effects in progeny of $sxt\Delta$ parents (Supplementary Data File 8). 56% of flies displayed an abnormal wing posture, either droopy wings or wings that were held out and up, and 52% of flies displayed etched tergites (Fig. 1c, top row, $n = 79$ flies). Consistent with the role of Idgfs in immune responses (Kucerova et al. 2016), a small percentage of adults (<5%) had lesions resembling melanotic clots, which normally occur at the sites of wounds or at sites of pathogen invasion (Fig. 1c, middle row, arrow). Although we have not quantified this change, we have noticed a decrease in the frequency of these melanotic lesions, potentially due to improved culture conditions or to the appearance of suppressors in the $sxt\Delta$/CyO strain. In addition, we found that on average, 30% of adult wings exhibited ectopic wing veins (Fig. 1c, bottom row, arrow, $n = 121$ wings), revealing defects in wing imaginal-disk patterning during larval and early pupal development. We observed a striking disparity between $sxt\Delta$ males (5% of wings) and $sxt\Delta$ females (74% of wings) displaying ectopic veins, potentially due to an X-chromosome suppressor.

Overall size of idgf mutant adults was not affected

As noted in the Introduction, CLPs have properties of growth factors (Shao et al. 2009; Lee et al. 2011; Areshkov et al. 2012). To assess whether loss of Idgfs compromises growth, we quantified fly size by measuring wing area, which correlates well with overall body size (Mirth and Shingleton 2012; Siomava et al. 2016). We compared average wing area in w^{1118} and $sxt\Delta$ adults. We found no significant difference between these genotypes under our culture conditions ($P = 0.65$, Student's t-test, $n = 20$ w^{1118} wings and 24 $sxt\Delta$ wings). Average wing area was ~1.5 mm^2 (Supplementary Data File 9) in flies, regardless of whether they had homozygous parents or parents carrying the CyO balancer, which expresses wild-type Idgfs. This result implies that these Idgfs do not contribute to growth and proliferation of imaginal disks and histoblast cells during larval and pupal development. Consistent with this hypothesis, we have not detected any defects in bristle morphology among the thousands of $sxt\Delta$ flies we have analyzed.

Dorsal appendage tube formation is disrupted in $sxt\Delta$ mutants

Cell migration, polarization, growth, proliferation, and signaling govern the tissue movements that form morphologic structures such as epithelial tubes. We used our DA tube morphogenesis model to assess the effects of Idgf loss of function during oogenesis (Fig. 2a). DA tubes produce eggshell structures that facilitate gas exchange for the developing embryo, and they are made by a subset of follicle cells in late-stage egg chambers. The egg chamber consists of 15 germline-derived nurse cells, 1 oocyte, and a surrounding monolayer of somatic epithelial cells consisting posteriorly of columnar cells and anteriorly of squamous cells (termed "stretch" cells). The tubes develop from 2 patches of precursor cells in the follicular epithelium and, through cell intercalation and cell shape change, elongate by migrating anteriorly over the stretch cells and beneath the extracellular matrix (Dorman et al. 2004; Ward and Berg 2005; Osterfield et al. 2013). The tube cells secrete eggshell protein into the tube lumen, providing a readout for tube formation, similar to the way a mold forms a sculpture (DAs; Fig. 2a, right image). This highly conserved process of tube formation is a wrapping mechanism akin to mammalian neural tube formation (Osterfield et al. 2017).

We previously observed disruption of DA morphogenesis using Idgf1 and Idgf3 overexpression (Zimmerman et al. 2017; Espinoza and Berg 2020) and Idgf RNAi for each single mutant (Zimmerman et al. 2017). Since null mutations are the gold standard in genetics, we asked "What about complete knockout of Idgfs?" We compared the DA phenotypes of eggs laid by each single Idgf CRISPR-null mutant and the $sxt\Delta$ mutant to the DAs of eggs laid by control (w^{1118}) flies and categorized the phenotypes as

mild, moderate, or severe by scoring the DAs while blinded to the genotypes (Fig. 2b). To limit the influence of potential background mutations, we assessed the phenotypes produced by single mutant genotypes *Idgf1Δ* through *Idgf6Δ* by placing each *Idgf*-deletion chromosome *in trans* to a deficiency chromosome generated independently by the Bloomington Stock Center (NIH P40OD018537; Ryder *et al.* 2004). Note that none of the deficiencies produced DA phenotypes on their own (Supplementary Table 3). The *sxtΔ* mutant was assessed homozygously due to the unfeasibility of creating flies heterozygous with deficiencies spanning each of the 6 deleted *Idgf* loci. Therefore, we cannot rule out the possibility that potential background mutations may influence homozygous *sxtΔ* embryonic and adult phenotypes.

Approximately 50% of eggs laid by the *sxtΔ* mutants and 18% of the *Idgf6Δ* mutants had moderate or severe phenotypes, but both of these percentages varied somewhat from experiment to experiment (see below). The other single mutants ($Idgf^{1Δ}$, $Idgf^{2Δ}$, $Idgf^{3Δ}$, $Idgf^{4Δ}$, and $Idgf^{5Δ}$) did not exhibit significant levels of defects [Fig. 2c (i)]. We also assessed the double mutant $Idgf^{2–3Δ}$ and the triple mutant $Idgf^{(1Δ,2–3Δ)}$ *in trans* to a deficiency uncovering the region. The triple mutant had a significant level of defects compared with eggs laid by w^{1118} flies ($P < 0.001$, Fisher's exact test). The double mutant did not have a significant level of defects ($P > 0.5$, Fisher's exact test; Supplementary Data File 10). Expression of an *Idgf6-GFP* transgene in a *sxtΔ* mutant background partially rescued the *sxtΔ* DA phenotype [Fig. 2c (ii) and Supplementary Data File 10].

Overall, these results provide evidence for important physiologic roles of Idgfs in tissue morphogenesis, potentially including cell polarization, migration, adhesion, and signaling.

Idgfs protect against effects of CO_2 exposure

While analyzing the DA defects in eggs laid by *Idgf* mutants, we observed variability in penetrance and expressivity. Initially, we found differences in the percentage and severity of DA defects for eggs laid by $Idgf^{6Δ}$ females. Because these 2 sets of experiments ($Idgf^{6Δ}$ vs other single *Idgf* mutants) were performed by 2 different lab workers, we asked whether these differences were biological or whether the variability was due to a difference in technique between lab workers (e.g. age of flies, overcrowding, or CO_2 exposure). Intriguingly, we determined that there was variability in whether flies were exposed to CO_2 when they were transferred to fresh egg-laying plates. This observation raised the question as to whether loss of *Idgf* function rendered flies more sensitive to CO_2.

To compare CO_2 sensitivity between wild-type and mutant flies, we assessed DA morphology on eggs laid by w^{1118} flies and *Idgf* mutants by using several different regimes of CO_2 exposure (Supplementary Data File 11). Treating adult females to 100% CO_2 for 60 s twice per day (~every 12 h) for 3.5 days (Supplementary Fig. 5a) resulted in a significant increase in DA defects on the eggs laid by $Idgf^{2Δ}$ through $Idgf^{6Δ}$ and *sxtΔ* mutants, but not on the w^{1118} eggs nor in $Idgf^{1Δ}$.

Since tissue and cellular responses to carbon dioxide depend on the length and severity of exposure (Helenius *et al.* 2009, 2016; Sharabi, Hurwitz, *et al.* 2009; Sharabi, Lecuona, *et al.* 2009), we asked if a prolonged exposure to a lower level of CO_2 would have a similar effect. We exposed *sxtΔ* mutant and w^{1118} adult flies to either 20% CO_2 or 100% air and evaluated DA morphology at 1.5–2 days and 7–8 days of exposure. Exposure to CO_2 over either of these time periods did not significantly increase DA defects in eggs laid by *sxtΔ* mutants (Supplementary Fig. 5b).

We next asked whether the effect of CO_2 exposure was directly due to the CO_2 itself or due to hypoxia, the transient absence of oxygen. To distinguish between these 2 hypotheses, we exposed flies to 100% N_2 for 5 min followed by DA analysis at 8–10 h and 2 days after exposure. We did not observe a significant effect on DA morphology following this treatment, indicating that the increase in DA morphology defects was directly due to CO_2 exposure rather than hypoxia (Fig. 3a).

These results suggest that Idgf proteins protect tissues against acute CO_2 exposure. If this hypothesis is correct, expression of Idgf protein should rescue the DA mutant phenotype associated with high CO_2. To test this prediction, we used a GFP-tagged transgene, *Idgf6-GFP*, in which Idgf6 is fused in-frame at its C-terminus to superfolder GFP (Sarov *et al.* 2016). We expressed this transgene in the $Idgf^{6Δ}$ and *sxtΔ* mutants and compared the DA phenotypes to the same mutants lacking the transgene. We exposed the flies to a single pulse of 100% CO_2 for 1 min and analyzed DA defects at 8–10 h and 2 days after exposure (Fig. 3b). While both mutants exhibited defects at 8–10 h after exposure, *Idgf6-GFP* expression restored the percentage of DA defects to pre-exposure levels in the $Idgf^{6Δ}$ mutants, and it reduced the DA defects in the *sxtΔ* mutants but not to the level of statistical significance. After 2 days, the DA defects in both mutants recovered to pre-exposure levels. These results demonstrate that this gene—environment interaction is due to the loss of Idgfs. Significantly, expression of a single Idgf protein can rescue or ameliorate the DA phenotype in *Idgf* mutants.

To examine the time course following acute CO_2 exposure on a finer scale, we exposed adult *sxtΔ* flies to a single pulse of 100% CO_2 for 1 min, followed by hourly DA defect analysis (Fig. 3c). Defects peaked at 6–10 h after exposure and then recovered by ~27 h after exposure.

In addition to the developmental roles for Idgfs in normoxia, these results support a hypothesis that Idgfs protect against morphogenetic disruption following acute CO_2 exposure.

Actin but not E-cadherin is disrupted in egg chambers after CO_2 exposure

How do Idgfs function in DA morphogenesis, and how does acute exposure to CO_2 impact that process? One hypothesis is that Idgfs are necessary for patterning the DA primordial cells. A second hypothesis is that Idgfs regulate cell morphology and epithelial tissue dynamics. To test these hypotheses, we exposed adult females to 100% CO_2 for 1 min and then waited for 20–30 min before dissecting, fixing, and staining the ovaries. We then examined patterning and cell morphology of the DA-forming cells using antibodies against Broad, a transcription factor that specifies the DA roof-forming cells, and against E-cadherin, an adhesion protein that outlines cell shapes (Dorman *et al.* 2004; Ward and Berg 2005; Ward *et al.* 2006).

Patterning was normal in both w^{1118} and *sxtΔ* in both the exposed and unexposed egg chambers as revealed by 2 patches of ~50, high-Broad-expressing cells residing just lateral to the dorsal midline (Fig. 4, a–c). Cell morphology in the DA patches, however, was more disorganized, and E-cadherin was more disrupted in the *sxtΔ* exposed egg chambers relative to the exposed w^{1118} and unexposed *sxtΔ* egg chambers (Fig. 4, a′–c′, rectangles). At Stage 12, DA roof-cell primordia were wider, and cells were less constricted in the *sxtΔ* mutants relative to the DA cells in the exposed w^{1118} egg chambers (Fig. 4, d and e, rectangles). After exposure to CO_2, *sxtΔ* DA-forming cells exhibited a reduction of filamentous actin from both the cell junctions and the basal surfaces (Fig. 4g). In contrast, cell shapes and actin levels looked normal in the w^{1118} DA-forming cells (Fig. 4f).

We quantified E-cadherin and actin in the DA-forming follicle cells by measuring fluorescent intensities across cell membranes using ImageJ (Fig. 5 and Supplementary Fig. 6) and calculating the total area under the plot profiles (supporting data are provided in Supplementary Data File 12). To assess whether potential differences in intensity might be stage or cell-type specific, we analyzed roof cells, floor cells, and main-body follicle cells at Stage 10B, just prior to tube wrapping, and at Stage 12, during tube elongation (Fig. 5a and Supplementary Fig. 6a). E-cadherin intensity was lower in $sxt\Delta$ mutants relative to w^{1118} control flies ($P \leq 0.05$), but it was not significantly affected by CO_2 exposure (Fig. 5, b and c and Supplementary Fig. 6b). In contrast, actin levels were similar in w^{1118} and $sxt\Delta$ mutants but dropped quickly in both samples upon exposure to CO_2 ($P \leq 0.05$; Fig. 5, b' and c' and Supplementary Fig. 6b'). These results suggest that Idgfs regulate E-cadherin expression or stability in normoxia and that they impact actin dynamics in response to CO_2.

Actin is disrupted in Stage 8–12 embryos after CO_2 exposure

To ask whether Idgfs regulate E-cadherin and actin in other contexts, we examined E-cadherin and actin during embryonic development. We exposed w^{1118} and $sxt\Delta$ embryos of all stages to 100%

CO_2 for 2 min before immediately dechorionating, fixing, and staining (Supplementary Data File 13). Since embryos comprise numerous distinct cell types, we focused on cells near the surface that were relatively uniform in size and easy to measure. We chose ectodermal cells located between the mid-lateral cells and lateral edge of the germ band in abdominal segments 2–6 and measured these cells during the extended germ band stages (late Stage 8–early Stage 12). Under these conditions, we observed no significant difference between E-cadherin levels in w^{1118} embryos or $sxt\Delta$ mutant embryos (Fig. 6, a and a'). Actin levels also did not differ significantly in w^{1118} embryos between treatments (Fig. 6, b and b'), but actin levels were significantly lower in $sxt\Delta$ mutants exposed to CO_2 compared with unexposed embryos. Taken together, these results support our hypothesis that CO_2 exposure disrupts actin in embryonic epithelia.

When analyzing actin dynamics in egg chambers, we noticed that some cell types were more sensitive to CO_2 exposure than others and that the effect of CO_2 exposure on actin perdured over a longer period in $sxt\Delta$ mutants compared with w^{1118} controls. We therefore asked whether we might see more dramatic effects in embryos if we exposed embryos during cellularization, a period when actin function is crucial (Sokac *et al.* 2022). We also reasoned that embryonic cells might be protected from CO_2
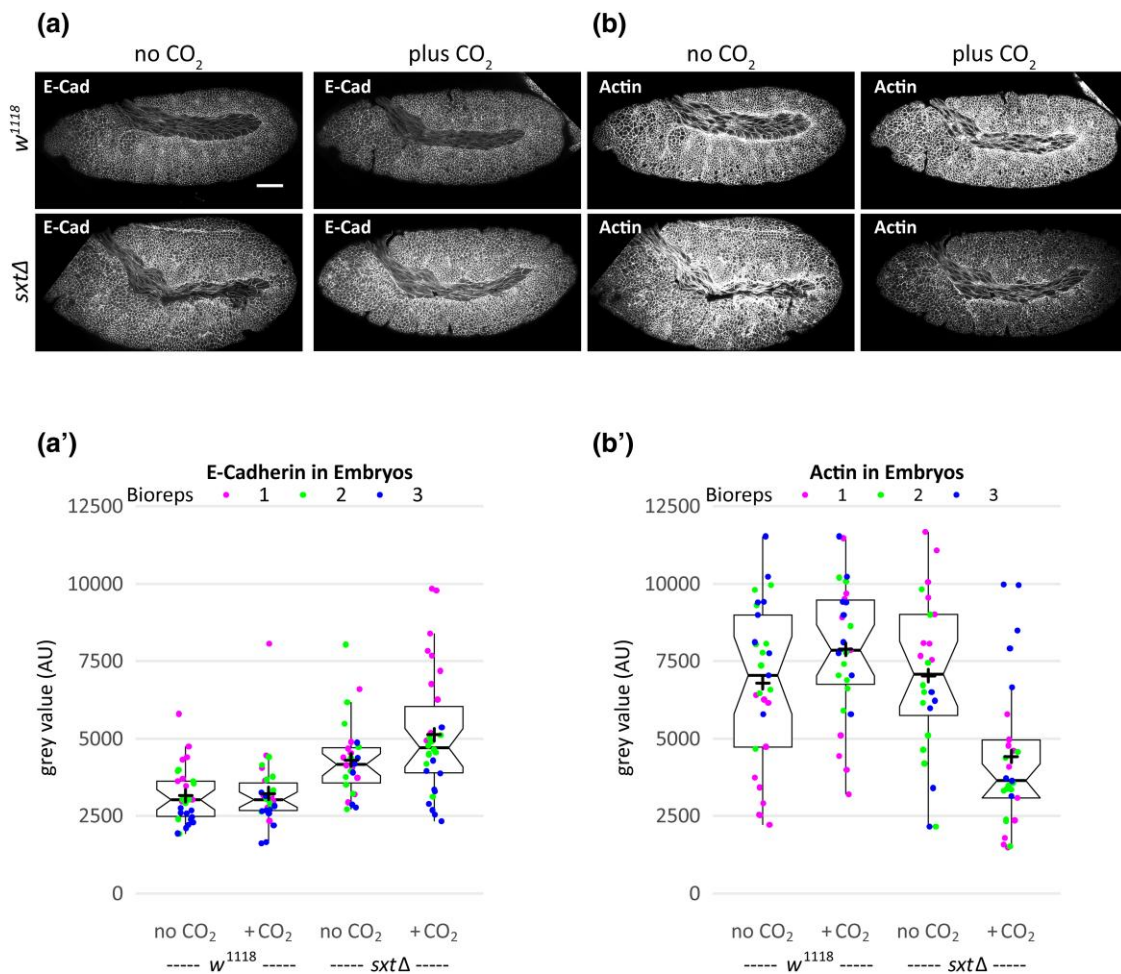
Fig. 6. Quantification of cortical actin and E-cadherin intensity in Stage 8–12 embryos. a, b) Representative embryo images showing E-cadherin (a) and actin (rhodamine phalloidin) (b) comparing genotypes and CO_2 regime as indicated. Scale bar = 50 μm. (a', b') Comparison of w^{1118} and $sxt\Delta$ fluorescence intensity measured across 6 cell membranes per embryo, from the center of 1 cell to the center of the neighboring cell. The colors represent different biological replicates. Each point in the graphs represents the average of the areas under the 6 plot profiles per embryo. The notches on the box plots represent the 95% confidence interval of the medians (horizontal lines), $\pm 1.57*$IQR/sqrt(n). IQR = interquartile range. + signs = means. Non-overlapping notches are strong evidence that their medians significantly differ. $sxt\Delta$ embryos are offspring of homozygous mutant parents.

exposure by the eggshell. We therefore exposed early stage embryos to 100% CO_2 and increased the exposure time to 6 min. In this experiment, embryos were allowed to age for 30 min before fixing them and staining with phalloidin. We measured actin fluorescence intensity across cell membranes in syncytial blastoderm embryos during Stages 3–5. Prior to cellularization in Stage 5, nuclei in the syncytial blastoderm embryo are surrounded by actin extensions (called pseudofurrows) at the periphery. In Stage 5, the actin furrows extend around the nuclei to form a single layer of cells surrounding the yolky core. At these stages, the cells are uniform in size and shape, facilitating uniformity in measurements. As we observed in egg chambers, loss of actin was significant in early embryos after exposure to CO_2 but did not differ significantly between w^{1118} and *sxtΔ* (Fig. 7, a–c; Supplementary Data File 14).

Discussion

We investigated the in vivo roles of *Drosophila* imaginal disk growth factors throughout development. Previous studies have sought to characterize the function of individual Idgfs using RNAi or in cell culture. We are the first to delete each of the *Idgf*s and develop fly lines with single or multiple deletions of the *Idgf*s, including flies null for all 6 *Idgf*s. Although individual knock-out strains lacked obvious visible defects, each Idgf could play roles in processes that enhance survival or fecundity under specific environmental conditions. These strains represent the first example of knocking out a complete gene family dispersed in the genome, and they offer the opportunity to explore the interplay between single gene functions and redundancy in a gene family. Using these tools, we found that loss of all Idgf function produces a variety of detrimental phenotypes.

In *Idgf sxtΔ* mutants, gonads form with significantly reduced germ cell numbers. Most germ cells are lost or die before they reach the somatic gonadal precursor cells, consistent with the low fertility we observed in *sxtΔ* adults. Normally, germ cells form at the posterior pole of the embryo and are taken into the midgut primordium during gastrulation. They initially form a tight cluster in the midgut, but subsequently extend protrusions toward the midgut cells, lose adhesion from each other, disperse, migrate individually through the midgut, and associate with somatic gonadal precursors cells to form the gonads (Review: Richardson and Lehmann 2010). To migrate, germ cells become polarized and extend protrusions toward the midgut cells. One
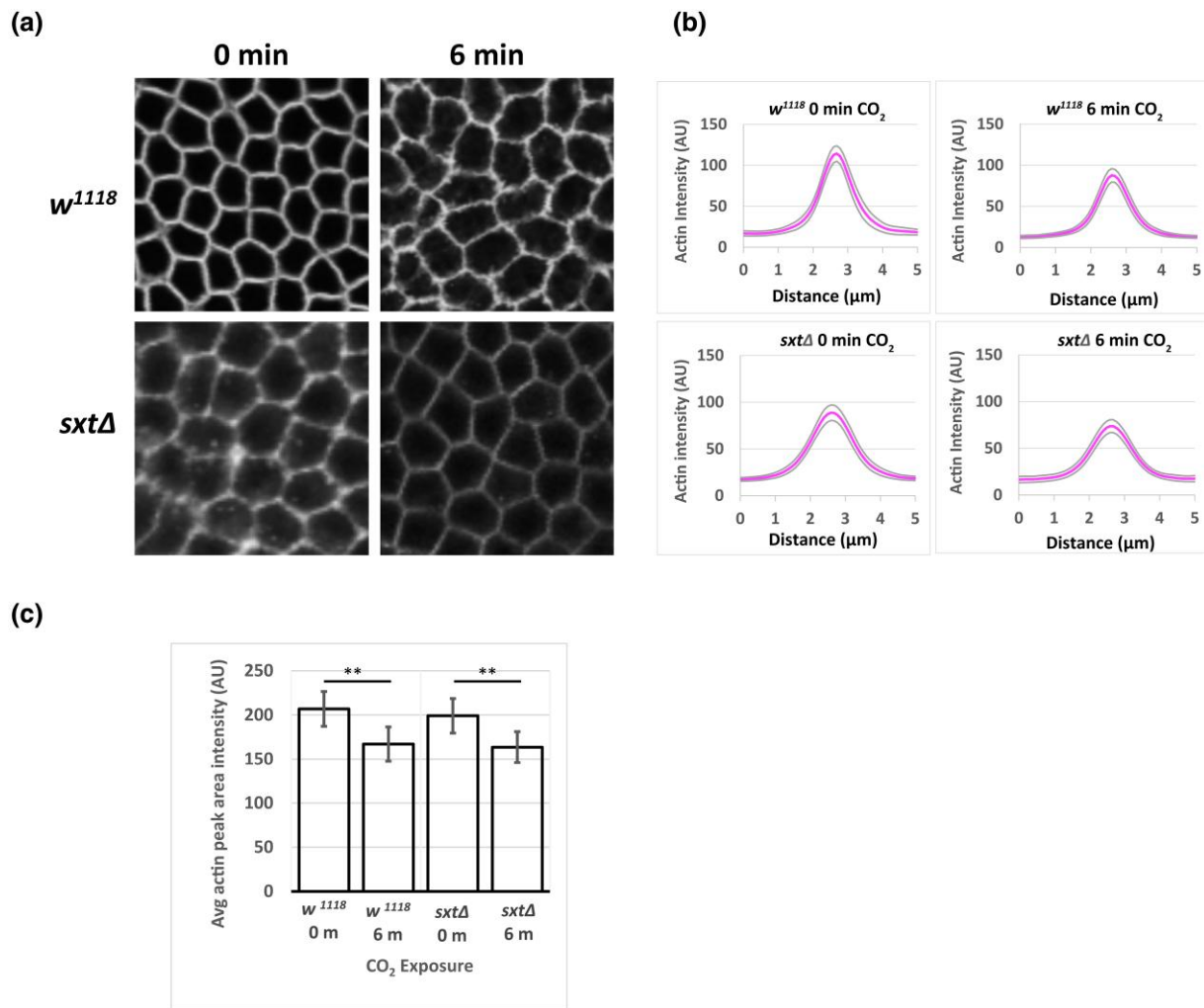
Fig. 7. Quantification of cortical actin intensity in Stage 3–5 embryos. a) Actin in early embryos comparing genotypes and CO_2 regime as indicated. b) Comparison of w^{1118} and *sxtΔ* fluorescence intensity plot profiles averaged across 6 cell membranes, from the center of 1 cell to the center of the neighboring cell, averaged over at least 10 Stage 3–5 embryos for each genotype and each exposure regime as indicated. Plots show mean (inner thicker plot line) and 95% confidence limits (outer thinner plot lines). c) Integrated area under the curves in (b) averaged over all measurements. *sxtΔ* embryos are offspring of homozygous mutant parents. Error bars show 95% confidence limits. **$P \le 0.01$, Student's *t*-test, Benjamini–Hochberg adjusted *P*-values.

hypothesis is that Idgfs participate in remodeling of cell junctions and actin dynamics in migrating cells, consistent with our finding that loss of all Idgfs disrupts E-cadherin and actin in certain contexts. A second hypothesis is that loss of Idgf function disrupts polarization and protrusiveness of primordial germ cells, consistent with a previous study demonstrating that Idgfs promote cell motility and protrusiveness in cell culture (Kawamura *et al.* 1999). Studies have identified key regulators of germ cell migration, such as the lipid phosphate phosphatases, Wunen and Wunen-2 (Hanyu-Nakamura *et al.* 2004), the small acidic protein, 14-3-3ε (Tsigkari *et al.* 2012), and pathways such as JAK/STAT (Li *et al.* 2003; Brown *et al.* 2006). CLPs are known to have properties of cytokines (Lee *et al.* 2011), raising the question of whether Idgfs may promote guidance cues for migrating germ cells. We have observed that Idgf6 associates with migrating germ cells from embryonic Stages 4–7; this association is lost by Stage 10. How Idgfs might interact with these components or otherwise participate in germ cell development will require further study.

Consistent with studies showing expression of Idgfs throughout development, we showed that hatch rates are severely reduced in *sxtΔ* homozygous embryos derived from *sxtΔ* parents. This effect of loss of all maternal and zygotic Idgfs was ameliorated by adding either maternal, zygotic, or both maternal and zygotically expressed Idgfs. Interestingly, offspring of parents where both parents carry a *CyO* chromosome in a *sxtΔ* background have a higher hatch rate than offspring of w^{1118} females crossed to *sxtΔ* males, even though in the second scenario, all embryos receive both maternal and zygotically expressed Idgfs while in the first scenario, 1 quarter of the offspring carry 2 balancers and another quarter lack zygotic Idgfs. Furthermore, w^{1118} females crossed to *sxtΔ* males lay more unfertilized or undeveloped embryos than w^{1118} females crossed to w^{1118} males. These results demonstrate that *sxtΔ* males are less fertile than their *sxtΔ/CyO* counterparts. One hypothesis is that the *sxtΔ* male's fertility is compromised by reduced numbers of germ cells in the gonad, consistent with our finding that germ-cell specification, migration, and/or survival is defective in *sxtΔ* embryos. We speculate that the small size of the ovaries in *sxtΔ* females may also result from defects in germ cell biology.

Further, we found that the proportions of homozygous vs heterozygous offspring produced by heterozygous parents deviate significantly from the expected Mendelian ratios, reflecting greater lethality of the homozygotes from embryonic through adult stages. Our observation that eclosion is delayed in *sxtΔ* mutants could imply that Idgfs function as growth hormones; loss of function could slow development. Nevertheless, we found no significant size difference between *Idgf* mutants and controls.

Consistent with disruption of embryonic development (as revealed by lower *sxtΔ* hatch rates), we observed abnormal expression of Engrailed protein and disorganized denticle belts in embryos, including a mislocalization of Engrailed at the cell membrane. Although secretion of Engrailed is well documented in some contexts (Joliot *et al.* 1998; Maizel *et al.* 2002; Punia *et al.* 2019), Engrailed functions as a transcription factor in the early embryo. Patterning is achieved through the expression of the segment polarity genes *wingless* (*wg*) and *engrailed* (*en*), which activates expression of *hedgehog* (*hh*). Within each segment, cells receiving the Wg signal produce smooth cuticle posteriorly, and cells receiving the Hh signal produce denticles anteriorly (Bejsovec and Martinez Arias 1991; Swarup and Verheyen 2012). The denticle-vs-smooth cell shapes are distinct: whereas the denticle-producing cells are rectangular and arranged in rows with the long edges oriented in the ventrolateral direction (similar to a staggered brick-wall arrangement), the smooth cells are larger and not arranged in rows (Hirano *et al.* 2009). Mislocalization or abnormal expression of En could cause a transformation of cell fate from non-denticle-producing to denticle-producing cells, resulting in the disorganized denticle belt phenotype we observed in *sxtΔ* embryos. Alternatively, cells in the epidermal epithelium may have altered cell adhesion and increased motility, allowing denticle-producing cells to invade into the non-denticle-producing cells.

Segmentation defects were apparent in adults in that *sxtΔ* flies exhibited etched tergites. Each abdominal segment in the adult epidermis develops from 3 bilateral pairs of groups of cells called histoblast nests. The anterior pair in each segment forms the tergite. Histoblast nests proliferate after pupariation and migrate by intercalation into the larval epithelial cells, which then extrude basally and die. The histoblast nests fuse and secrete the adult cuticle (Mangione and Martin-Blanco 2018; Nardi *et al.* 2018; Michel and Dahmann 2020; Prat-Rojo *et al.* 2020; Athilingam *et al.* 2021; Panzade and Matis 2021; Davis *et al.* 2022). Successful migration depends on Decapentaplegic (Dpp) and protrusive extensions at the leading edge of the histoblast nests (Ninov *et al.* 2007, 2010). Our findings suggest a role for Idgfs in histoblast cell proliferation, migration, or survival, but how Idgfs function in tergite formation is unknown.

Our previous studies showed that the stretch cells relay signals from the nurse cells to the DA cells to guide their movement and ensure tube closure. These signals rely on function of the SOX transcription factor Bullwinkle (Bwk) in the nurse cells (Rittenhouse dissertation, 1996. Bullwinkle, an HMG box protein, is required for proper development during oogenesis, embryogenesis and metamorphosis in *Drosophila melanogaster*, PhD, University of Washington) (Rittenhouse and Berg 1995), and the non-receptor tyrosine kinases Shark and Src42a in the stretch cells (Tran and Berg 2003). The specific signaling molecules and their targets are unknown. *Bwk* mutants produce short, wide, open tubes that create DAs resembling moose antlers (Rittenhouse and Berg 1995; Dorman *et al.* 2004). Shark and Src42A act downstream of Bwk to regulate DA morphogenesis; Shark loss of function enhances the Bwk phenotype (Tran and Berg 2003).

In this study, we found that except for *Idgf6*, the single *Idgf*-null mutants did not cause a defective DA phenotype. The results for the single null mutants contrast with our previous studies using RNAi to knock down each *Idgf* individually (Zimmerman *et al.* 2017); we found that RNAi knockdown of each *Idgf* results in a partially penetrant DA phenotype featuring shorter, wider DAs. Shorter, wider DAs also occur when Idgfs are overexpressed or when elevated as in eggs from *bwk* mutant flies. Such "moose antler" DAs contrast with the moderate category of defective DAs in the null mutants, which have thin DAs. This result suggests that tissue-specific RNAi knockdown of single Idgfs actually induces a compensation process that over-expresses Idgfs, producing a gain-of-function phenotype.

Why do significant defects occur in single *Idgf* RNAi knockdowns, but not in single nulls? One difference in these scenarios is that RNAi knockdown is spatially and temporally restricted, occurring in a short window at precisely the time that DA tubes are formed (see below). In contrast, the deletions remove gene function throughout development, allowing a more balanced homeostasis process to occur. Functional redundancy from the remaining Idgfs or even from expression of non-*Idgf* genes could account for the incomplete penetrance or lack of a phenotype. Duplicated genes can maintain functional redundancy despite their divergence over evolutionary time (Dean *et al.* 2008;

DeLuna *et al.* 2008; Kafri *et al.* 2008; Musso *et al.* 2008). Functional redundancy between paralogous genes can result in a strong phenotype when all of the paralogs are deleted and a weak or neutral phenotype when the genes are deleted singly (Gu *et al.* 2003; Dean *et al.* 2008; DeLuna *et al.* 2008; Kafri *et al.* 2008; Musso *et al.* 2008), similar to what we observed for the *Idgf* null mutants.

Compensation in single null mutants from the remaining wild-type paralogs or even from non-*Idgf* genes could be post-transcriptional, e.g. through increased translation or greater protein stability. Compensation may also occur through transcriptional adaptation, in which upregulation of compensating genes can be triggered by any of a number of mRNA decay pathways that target aberrant mRNAs (Garneau *et al.* 2007). A recent study demonstrated that transcriptional adaptation depends on the existence of a mutant mRNA, for which degradation can occur via different surveillance pathways, including non-stop, no-go, or non-sense-mediated decay, depending on the nature of the mutation. Upregulation can then occur in genes with sequence similarity to the degraded mRNA (Garneau *et al.* 2007; Rossi *et al.* 2015; El-Brolosy and Stainier 2017; El-Brolosy *et al.* 2019).

Except for *Idgf²ᴬ*, the single null mutants cannot express a transcript. The *Idgf2* deletion leaves intact the 5′-UTR, the first exon and intron, and part of the second exon, potentially allowing production of a mutant transcript and therefore transcriptional adaptation in the *Idgf²ᴬ* and *sxtΔ* mutants, which carry the *Idgf2* deletion. Degradation of the *Idgf²ᴬ* transcript could not be via the non-sense-mediated decay (NMD) process, which requires a premature stop codon upstream of an intron. Degradation via a non-NMD pathway, however, could be occurring in either the *Idgf²ᴬ* or *sxtΔ* mutant lines. Our RNAi experiments were performed in a wild-type background, so there would be no mutant mRNAs, and any adaptation would be on the translational or post-translational protein level (Torres *et al.* 2008; DeLuna *et al.* 2010; Donnelly and Storchova 2014; Ishikawa *et al.* 2017).

Although adaptation could be occurring in both the nulls and the knockdowns, the time frame for adaptation could also be a factor. In the RNAi study, we used the *GAL4/UAS* system to knockdown transcripts from each of the *Idgf* genes. We used a stretch-cell-specific Gal4 driver, which is not expressed until Stage 10 of egg chamber development, after patterning has occurred but just hours before tube formation. This timing may not allow enough time for optimal compensation to occur. On the other hand, *Idgf*-null mutant flies are mutant throughout their entire life cycle. Thus, the different results of our *Idgf* RNAi knockdown and null experiments could be due to different mechanisms of compensation. Discerning whether compensation is occurring and what contributes to the differences in phenotypes exhibited by overexpression, RNAi, and gene deletion will require further study.

Mutations can render cells less robust to endogenous or exogenous perturbations (Levy and Siegal 2008; Masel and Siegal 2009). *Drosophila* researchers commonly use CO_2 to anesthetize flies without considering the potential profound and long-lasting effects of CO_2 exposure. Previous studies have shown that hypercapnia can suppress the immune system and alter gene expression via the NF-κB pathway in mammalian cells (Cummins *et al.* 2010). Hypercapnia also reduces fertility (Helenius *et al.* 2009) and alters climbing and flight behavior in *Drosophila* (Bartholomew *et al.* 2015).

We demonstrated that exposing *Idgf*-null mutants to CO_2 enhances DA morphogenesis defects independently of hypoxia and induces loss of cortical actin in epithelial tissues during oogenesis and embryonic development. We did note molecular differences, raising the question of whether Idgfs regulate E-cadherin in

normoxia and actin in response to CO_2. We saw that E-cadherin was disrupted in *sxtΔ* mutant egg chambers but was unaffected by CO_2 exposure in either egg chambers or embryos. In contrast, actin levels were unaffected in *sxtΔ* mutants vs controls, and they were significantly reduced upon CO_2 exposure in both strains (Figs. 5 and 7). Nevertheless, DA tubes proceeded to develop normally in the control but not in the *sxtΔ* mutants (Figs. 3c and 5a). It could be that the actin is also perturbed in wild-type tissue but recovers, whereas absence of Idgfs eliminates a similar recovery in *sxtΔ* tissue. The mechanisms leading to these novel outcomes are unknown.

One possible mechanism for this regulation is that Idgfs interact with the immune deficiency (IMD) pathway through the transcription factor Relish (*Drosophila* NF-κB). Previous studies show that Relish inhibits JNK signaling (Park *et al.*, 2004). Activation of JNK signaling reorganizes the actin cytoskeleton, impacting developmental processes such as cell migration and dorsal closure (Jacinto *et al.* 2000; Kockel *et al.* 2001; Kaltschmidt *et al.* 2002; Homsy *et al.* 2006; Rudrapatna *et al.* 2014). Upon Relish loss, JNK activation causes upregulation of actin remodelers (Ramesh *et al.* 2021). Another possibility is that CO_2 exposure reduces pH at the cell membrane, thereby altering actin dynamics. pH is an important regulator in developmental processes such as differentiation (Ulmschneider *et al.* 2016) and tissue architecture (Grillo-Hill *et al.* 2015). Alternatively, the mechanism could involve a pathway independent of JNK signaling or pH.

A common thread among the various phenotypes produced by loss of all Idgfs is the disruption of E-cadherin and actin, an outcome that could interfere with cell migration, segmentation, and tissue morphogenesis. Consistent with this hypothesis, we recently identified *eukaryotic translation initiation factor 3 subunit e* (*eIF3e*) as a strong enhancer of *Idgf3* overexpression (Espinoza and Berg 2020). eIF3e is part of a complex that regulates the redox enzyme, Mical, which functions to disassemble actin filaments and inhibit actin polymerization (Hung *et al.* 2010; Grintsevich *et al.* 2016, 2017, 2021). We are currently investigating the mechanistic role of Idgfs in this pathway.

Our investigation into the effects of complete loss of Idgfs has raised intriguing questions regarding Idgf function. What are the pathways? What are the precise mechanisms? What are the common threads among the various phenotypes? Our *Idgf* null lines are valuable tools that will facilitate studies providing new insights into the function of Idgfs in *Drosophila*. Our results suggest new avenues of investigation for the mechanisms of CLP function in cancer pathogenesis, autoimmune disease, and tissue remodeling disorders.

Data availability

Fly lines generated in our lab are available upon request. Sequences confirming the extent and structure of the *Idgf* deletions are available in GenBank (accession numbers OP745290–OP745323, release date 2022 December 14). The authors affirm that all other data necessary for confirming the conclusions of the article are present within the article, figures, tables, and in the supplementary data files: Data Files S1 through S16. Data File S1 contains hatch rate data, Data File S2 contains larval and pupal lethality data, Data File S3 contains eclosion data, Data File S4 contains number-of-eggs-laid data, Data File S5 contains germ-cell counts, Data File S6 contains counts of embryos with Engrailed at the cell membranes, Data File S7 contains disorganized-denticle-belt counts, Data File S8 contains adult cuticle-defect data, Data File S9 contains wing-area

measurements, Data File S10 contains dorsal-appendage defect and rescue data, Data File S11 contains hypoxia and CO_2 exposure data, Data File S12 contains quantification of actin and E-cadherin in egg chambers, Data File S13 contains quantification of actin and E-cadherin in Stage 3–5 embryos, Data File S14 contains quantification of actin and E-cadherin in Stage 8–11 embryos, Data File S15 contains *sxt∆* fertility data, and Data File S16 contains descriptions of the GenBank sequences.

Supplemental material available at GENETICS online.

Conflicts of interest statement

The authors declare no conflict of interest.

Author contributions

C.A.B.: Project design; oversight of all experiments; analyses of mutant embryos and adult fertility; review and editing of manuscript.

L.G.S.: Generation of *Idgf6∆* fly strain using CRISPR/Cas9; experiments and data analysis to examine *Idgf6∆* DA defects; experiments to assess variability in phenotypes; review of manuscript.

A.E.S.: Generation of *Idgf* null fly strains using CRISPR/Cas9; experiments (hatch rates, DA morphogenesis, adult phenotype analysis, germ-cell migration phenotype, CO_2 response in egg chambers, patterning in egg chambers, actin, and E-cadherin measurements in egg chambers); imaging; data analyses; review of manuscript.

S.G.Z.: Writing and editing drafts, constructing figures, experiments (E-cadherin and actin in embryos, hatch rates, larval and pupal lethality, adult cuticle phenotypes, wing area measurements, embryonic and larval denticles, IHC, and phalloidin in embryos), imaging, and data analysis.

Literature cited

Areshkov PO, Avdieiev SS, Balynska OV, Leroith D, Kavsan VM. Two closely related human members of chitinase-like family, CHI3L1 and CHI3L2, activate ERK1/2 in 293 and U373 cells but have the different influence on cell proliferation. Int J Biol Sci. 2012;8(1):39–48. doi:10.7150/ijbs.8.39.

Arias EB, Verhage HG, Jaffe RC. Complementary deoxyribonucleic acid cloning and molecular characterization of an estrogen-dependent human oviductal glycoprotein. Biol Reprod. 1994;51(4):685–694. doi:10.1095/biolreprod51.4.685.

Athilingam T, Tiwari P, Toyama Y, Saunders TE. Mechanics of epidermal morphogenesis in the *Drosophila* pupa. Semin Cell Dev Biol. 2021;120:171–180. doi:10.1016/j.semcdb.2021.06.008.

Bartholomew NR, Burdett JM, VandenBrooks JM, Quinlan MC, Call GB. Impaired climbing and flight behaviour in *Drosophila melanogaster* following carbon dioxide anaesthesia. Sci Rep. 2015;5(1):15298. doi:10.1038/srep15298.

Bejsovec A, Martinez Arias A. Roles of wingless in patterning the larval epidermis of *Drosophila*. Development. 1991;113(2):471–485. doi:10.1242/dev.113.2.471.

Brown S, Zeidler MP, Hombria JE. JAK/STAT signalling in *Drosophila* controls cell motility during germ cell migration. Dev Dyn. 2006;235(4):958–966. doi:10.1002/dvdy.20709.

Broz V, Kucerova L, Rouhova L, Fleischmannova J, Strnad H, Bryant PJ, Zurovec M. Drosophila imaginal disc growth factor 2 is a trophic factor involved in energy balance, detoxification, and innate immunity. Sci Rep. 2017;7(1):43273. doi:10.1038/srep43273.

Bussink AP, Speijer D, Aerts JM, Boot RG. Evolution of mammalian chitinase(-like) members of family 18 glycosyl hydrolases. Genetics. 2007;177(2):959–970. doi:10.1534/genetics.107.075846.

Carton Y, Nappi AJ. Immunogenetic aspects of the cellular immune response of *Drosophilia* against parasitoids. Immunogenetics. 2001;52(3-4):157–164. doi:10.1007/s002510000272.

Cummins EP, Oliver KM, Lenihan CR, Fitzpatrick SF, Bruning U, Scholz CC, Slattery C, Leonard MO, McLoughlin P, Taylor CT. NF-κB links CO_2 sensing to innate immunity and inflammation in mammalian cells. J Immunol. 2010;185(7):4439–4445. doi:10.4049/jimmunol.1000701.

Davis JR, Ainslie AP, Williamson JJ, Ferreira A, Torres-Sanchez A, Hoppe A, Mangione F, Smith MB, Martin-Blanco E, Salbreux G, et al. ECM Degradation in the *Drosophila* abdominal epidermis initiates tissue growth that ceases with rapid cell-cycle exit. Curr Biol. 2022;32(6):1285–1300.e4. doi:10.1016/j.cub.2022.01.045.

Dean EJ, Davis JC, Davis RW, Petrov DA. Pervasive and persistent redundancy among duplicated genes in yeast. PLoS Genet. 2008;4(7):e1000113. doi:10.1371/journal.pgen.1000113.

DeLuna A, Springer M, Kirschner MW, Kishony R. Need-based up-regulation of protein levels in response to deletion of their duplicate genes. PLoS Biol. 2010;8(3):e1000347. doi:10.1371/journal.pbio.1000347.

DeLuna A, Vetsigian K, Shoresh N, Hegreness M, Colon-Gonzalez M, Chao S, Kishony R. Exposing the fitness contribution of duplicated genes. Nat Genet. 2008;40(5):676–681. doi:10.1038/ng.123.

Dilks SA, DiNardo S. Non-cell-autonomous control of denticle diversity in the *Drosophila* embryo. Development. 2010;137(8):1395–1404. doi:10.1242/dev.045450.

DiNardo S, Kuner JM, Theis J, O'Farrell PH. Development of embryonic pattern in *D. melanogaster* as revealed by accumulation of the nuclear engrailed protein. Cell. 1985;43(1):59–69. doi:10.1016/0092-8674(85)90012-1.

Di Rosa M, Distefano G, Zorena K, Malaguarnera L. Chitinases and immunity: ancestral molecules with new functions. Immunobiology. 2016;221(3):399–411. doi:10.1016/j.imbio.2015.11.014.

Donnelly N, Storchova Z. Dynamic karyotype, dynamic proteome: buffering the effects of aneuploidy. Biochim Biophys Acta. 2014;1843(2):473–481. doi:10.1016/j.bbamcr.2013.11.017.

Dorman JB, James KE, Fraser SE, Kiehart DP, Berg CA. *Bullwinkle* is required for epithelial morphogenesis during *Drosophila* oogenesis. Dev Biol. 2004;267(2):320–341. doi:10.1016/j.ydbio.2003.10.020.

Dougan S, DiNardo S. *Drosophila* wingless generates cell type diversity among engrailed expressing cells. Nature. 1992;360(6402): 347–350. doi:10.1038/360347a0.

El-Brolosy MA, Kontarakis Z, Rossi A, Kuenne C, Günther S, Fukuda N, Kikhi K, Boezio GLM, Takacs CM, Lai S-L, *et al.* Genetic compensation triggered by mutant mRNA degradation. Nature. 2019;568-(7751):193–197. doi:10.1038/s41586-019-1064-z.

El-Brolosy MA, Stainier DYR. Genetic compensation: a phenomenon in search of mechanisms. PLoS Genet. 2017;13(7):e1006780. doi: 10.1371/journal.pgen.1006780.

Espinoza CY, Berg CA. Detecting new allies: modifier screen identifies a genetic interaction between imaginal disc growth factor 3 and combover, a rho-kinase substrate, during dorsal appendage tube formation in *Drosophila*. G3 (Bethesda). 2020;10(10): 3585–3599. doi:10.1534/g3.120.401476.

Francescone RA, Scully S, Faibish M, Taylor SL, Oh D, Moral L, Yan W, Bentley B, Shao R. Role of YKL-40 in the angiogenesis, radioresistance, and progression of glioblastoma. J Biol Chem. 2011;286(17): 15332–15343. doi:10.1074/jbc.M110.212514.

Fuhrman JA, Lane WS, Smith RF, Piessens WF, Perler FB. Transmission-blocking antibodies recognize microfilarial chitinase in brugian lymphatic filariasis. Proc Natl Acad Sci U S A. 1992;89(5): 1548–1552. doi:10.1073/pnas.89.5.1548.

Fusetti F, Pijning T, Kalk KH, Bos E, Dijkstra BW. Crystal structure and carbohydrate-binding properties of the human cartilage glycoprotein-39. J Biol Chem. 2003;278(39):37753–37760. doi:10. 1074/jbc.M303137200.

Garneau NL, Wilusz J, Wilusz CJ. The highways and byways of mRNA decay. Nat Rev Mol Cell Biol. 2007;8(2):113–126. doi:10.1038/ nrm2104.

Grillo-Hill BK, Choi C, Jimenez-Vidal M, Barber DL. Increased H(+) efflux is sufficient to induce dysplasia and necessary for viability with oncogene expression. Elife. 2015;4:e03270. doi:10.7554/ eLife.03270.

Grintsevich EE, Ahmed G, Ginosyan AA, Wu H, Rich SK, Reisler E, Terman JR. Profilin and Mical combine to impair F-actin assembly and promote disassembly and remodeling. Nat Commun. 2021; 12(1):5542. doi:10.1038/s41467-021-25781-3.

Grintsevich EE, Ge P, Sawaya MR, Yesilyurt HG, Terman JR, Zhou ZH, Reisler E. Catastrophic disassembly of actin filaments via Mical-mediated oxidation. Nat Commun. 2017;8(1):2183. doi:10. 1038/s41467-017-02357-8.

Grintsevich EE, Yesilyurt HG, Rich SK, Hung RJ, Terman JR, Reisler E. F-actin dismantling through a redox-driven synergy between Mical and cofilin. Nat Cell Biol. 2016;18(8):876–885. doi:10.1038/ ncb3390.

Gu Z, Steinmetz LM, Gu X, Scharfe C, Davis RW, Li WH. Role of duplicate genes in genetic robustness against null mutations. Nature. 2003;421(6918):63–66. doi:10.1038/nature01198.

Guan R, Lin R, Jin R, Lu L, Liu X, Hu S, Sun L. Chitinase-like protein YKL-40 regulates human bronchial epithelial cells proliferation, apoptosis, and migration through TGF-beta1/Smads pathway. Hum Exp Toxicol. 2020;39(4):451–463. doi:10.1177/ 0960327119891218.

Hanyu-Nakamura K, Kobayashi S, Nakamura A. Germ cell-autonomous Wunen2 is required for germline development in *Drosophila* embryos. Development. 2004;131(18):4545–4553. doi:10.1242/dev.01321.

He CH, Lee CG, Dela Cruz CS, Lee C-M, Zhou Y, Ahangari F, Ma B, Herzog EL, Rosenberg SA, Li Y, *et al.* Chitinase 3-like 1 regulates

cellular and tissue responses via IL-13 receptor alpha2. Cell Rep. 2013;4(4):830–841. doi:10.1016/j.celrep.2013.07.032.

Helenius IT, Haake RJ, Kwon Y-J, Hu JA, Krupinski T, Casalino-Matsuda SM, Sporn PHS, Sznajder JI, Beitel GJ. Identification of *Drosophila* Zfh2 as a mediator of hypercapnic immune regulation by a genome-wide RNA interference screen. J Immunol. 2016; 196(2):655–667. doi:10.4049/jimmunol.1501708.

Helenius IT, Krupinski T, Turnbull DW, Gruenbaum Y, Silverman N, Johnson EA, Sporn PHS, Sznajder JI, Beitel GJ. Elevated CO_2 suppresses specific *Drosophila* innate immune responses and resistance to bacterial infection. Proc Natl Acad Sci U S A. 2009; 106(44):18710–18715. doi:10.1073/pnas.0905925106.

Hirano M, Neff D, Collier S. Cell shape and epithelial patterning in the *Drosophila* embryonic epidermis. Fly (Austin). 2009;3(3):185–191. doi:10.4161/fly.3.3.9138.

Homsy JG, Jasper H, Peralta XG, Wu H, Kiehart DP, Bohmann D. JNK signaling coordinates integrin and actin functions during *Drosophila* embryogenesis. Dev Dyn. 2006;235(2):427–434. doi:10. 1002/dvdy.20649.

Hu B, Trinh K, Figueira WF, Price PA. Isolation and sequence of a novel human chondrocyte protein related to mammalian members of the chitinase protein family. J Biol Chem. 1996; 271(32):19415–19420. doi:10.1074/jbc.271.32.19415.

Hung R-J, Yazdani U, Yoon J, Wu H, Yang T, Gupta N, Huang Z, van Berkel Willem JH, Terman JR. Mical links semaphorins to F-actin disassembly. Nature. 2010;463(7282):823–827. doi:10. 1038/nature08724.

Irving P, Troxler L, Heuer TS, Belvin M, Kopczynski C, Reichhart J-M, Hoffmann JA, Hetru C. A genome-wide analysis of immune responses in *Drosophila*. Proc Natl Acad Sci U S A. 2001;98(26): 15119–15124. doi:10.1073/pnas.261573998.

Ishikawa K, Makanae K, Iwasaki S, Ingolia NT, Moriya H. Post-translational dosage compensation buffers genetic perturbations to stoichiometry of protein complexes. PLoS Genet. 2017;13(1):e1006554. doi:10.1371/journal.pgen.1006554.

Jacinto A, Wood W, Balayo T, Turmaine M, Martinez-Arias A, Martin P. Dynamic actin-based epithelial adhesion and cell matching during *Drosophila* dorsal closure. Curr Biol. 2000;10(22): 1420–1426. doi:10.1016/S0960-9822(00)00796-X.

Joliot A, Maizel A, Rosenberg D, Trembleau A, Dupas S, Volovitch M, Prochiantz A. Identification of a signal sequence necessary for the unconventional secretion of Engrailed homeoprotein. Curr Biol. 1998;8(15):856–863. doi:10.1016/S0960-9822(07)00346-6.

Kafri R, Dahan O, Levy J, Pilpel Y. Preferential protection of protein interaction network hubs in yeast: evolved functionality of genetic redundancy. Proc Natl Acad Sci U S A. 2008;105(4):1243–1248. doi:10.1073/pnas.0711043105.

Kaltschmidt JA, Lawrence N, Morel V, Balayo T, Fernandez BG, Pelissier A, Jacinto A, Martinez Arias A. Planar polarity and actin dynamics in the epidermis of *Drosophila*. Nat Cell Biol. 2002;4(12): 937–944. doi:10.1038/ncb882.

Kawamura K, Shibata T, Saget O, Peel D, Bryant PJ. A new family of growth factors produced by the fat body and active on *Drosophila* imaginal disc cells. Development. 1999;126(2): 211–219. doi:10.1242/dev.126.2.211.

Khush RS, Lemaitre B. Genes that fight infection: what the *Drosophila* genome says about animal immunity. Trends Genet. 2000;16(10): 442–449. doi:10.1016/S0168-9525(00)02095-3.

Kidwell JF. The effective lethal phase of the curly mutant in *Drosophila melanogaster*. J Hered. 1972;63(2):100. doi:10.1093/ oxfordjournals.jhered.a108225.

Kirkpatrick RB, Matico RE, McNulty DE, Strickler JE, Rosenberg M. An abundantly secreted glycoprotein from *Drosophila melanogaster* is

related to mammalian secretory proteins produced in rheumatoid tissues and by activated macrophages. Gene. 1995;153(2):147–154. doi:10.1016/0378-1119(94)00756-I.

Kockel L, Homsy JG, Bohmann D. Drosophila AP-1: lessons from an invertebrate. Oncogene. 2001;20(19):2347–2364. doi:10.1038/sj.onc.1204300.

Kucerova L, Broz V, Arefin B, Maaroufi HO, Hurychova J, Strnad H, Zurovec M, Theopold U. The *Drosophila* chitinase-like protein IDGF3 is involved in protection against nematodes and in wound healing. J Innate Immun. 2016;8(2):199–210. doi:10.1159/000442351.

Kzhyshkowska J, Gratchev A, Martens J-H, Pervushina O, Mamidi S, Johansson S, Schledzewski K, Hansen B, He X, Tang J, *et al.* Stabilin-1 localizes to endosomes and the trans-Golgi network in human macrophages and interacts with GGA adaptors. J Leukoc Biol. 2004;76(6):1151–1161. doi:10.1189/jlb.0504300.

Kzhyshkowska J, Mamidi S, Gratchev A, Kremmer E, Schmuttermaier C, Krusell L, Haus G, Utikal J, Schledzewski K, Scholtze J, *et al.* Novel stabilin-1 interacting chitinase-like protein (SI-CLP) is up-regulated in alternatively activated macrophages and secreted via lysosomal pathway. Blood. 2006;107(8):3221–3228. doi:10.1182/blood-2005-07-2843.

Kzhyshkowska J, Yin S, Liu T, Riabov V, Mitrofanova I. Role of chitinase-like proteins in cancer. Biol Chem. 2016;397(3):231–247. doi:10.1515/hsz-2015-0269.

LeBlanc MG, Lehmann R. Domain-specific control of germ cell polarity and migration by multifunction Tre1 GPCR. J Cell Biol. 2017;216(9):2945–2958. doi:10.1083/jcb.201612053.

Lee CG, Da Silva CA, Dela Cruz CS, Ahangari F, Ma B, Kang M-J, He C-H, Takyar S, Elias JA. Role of chitin and chitinase/chitinase-like proteins in inflammation, tissue remodeling, and injury. Annu Rev Physiol. 2011;73(1):479–501. doi:10.1146/annurev-physiol-012110-142250.

Levy SF, Siegal ML. Network hubs buffer environmental variation in *Saccharomyces cerevisiae*. PLoS Biol. 2008;6(11):e264. doi:10.1371/journal.pbio.0060264.

Li J, Xia F, Li WX. Coactivation of STAT and Ras is required for germ cell proliferation and invasive migration in *Drosophila*. Dev Cell. 2003;5(5):787–798. doi:10.1016/S1534-5807(03)00328-9.

Libreros S, Garcia-Areas R, Keating P, Carrio R, Iragavarapu-Charyulu VL. Exploring the role of CHI3L1 in "pre-metastatic" lungs of mammary tumor-bearing mice. Front Physiol. 2013;4:392. doi:10.3389/fphys.2013.00392.

Liu N, Han H, Lasko P. Vasa promotes *Drosophila* germline stem cell differentiation by activating mei-P26 translation by directly interacting with a (U)-rich motif in its 3′ UTR. Genes Dev. 2009;23(23):2742–2752. doi:10.1101/gad.1820709.

Low D, Subramaniam R, Lin L, Aomatsu T, Mizoguchi A, Ng A, DeGruttola AK, Lee CG, Elias JA, Ando h Akira, *et al.* Chitinase 3-like 1 induces survival and proliferation of intestinal epithelial cells during chronic inflammation and colitis-associated cancer by regulating S100A9. Oncotarget. 2015;6(34):36535–36550. doi:10.18632/oncotarget.5440.

Lu Y, Chang N, Zhao X, Xue R, Liu J, Yang L, Li L. Activated neutrophils secrete chitinase-like 1 and attenuate liver inflammation by inhibiting pro-inflammatory macrophage responses. Front Immunol. 2022;13:824385. doi:10.3389/fimmu.2022.824385.

Maizel A, Tassetto M, Filhol O, Cochet C, Prochiantz A, Joliot A. Engrailed homeoprotein secretion is a regulated process. Development. 2002;129(15):3545–3553. doi:10.1242/dev.129.15.3545.

Malik P, Chaudhry N, Mittal R, Mukherjee TK. Role of receptor for advanced glycation end products in the complication and progression of various types of cancers. Biochim Biophys Acta. 2015;1850(9):1898–1904. doi:10.1016/j.bbagen.2015.05.020.

Mangione F, Martin-Blanco E. The dachsous/fat/four-jointed pathway directs the uniform axial orientation of epithelial cells in the *Drosophila* abdomen. Cell Rep. 2018;25(10):2836–2850.e4. doi:10.1016/j.celrep.2018.11.036.

Masel J, Siegal ML. Robustness: mechanisms and consequences. Trends Genet. 2009;25(9):395–403. doi:10.1016/j.tig.2009.07.005.

Mazur M, Zielinska A, Grzybowski MM, Olczak J, Fichna J. Chitinases and chitinase-like proteins as therapeutic targets in inflammatory diseases, with a special focus on inflammatory bowel diseases. Int J Mol Sci. 2021;22(13):6966. doi:10.3390/ijms22136966.

Meister M, Hetru C, Hoffmann JA. The antimicrobial host defense of *Drosophila*. Curr Top Microbiol Immunol. 2000;248:17–36. doi:10.1007/978-3-642-59674-2_2.

Meng G, Zhao Y, Bai X, Liu Y, Green TJ, Luo Ming, Zheng X. Structure of human stabilin-1 interacting chitinase-like protein (SI-CLP) reveals a saccharide-binding cleft with lower sugar-binding selectivity. J Biol Chem. 2010;285(51):39898–39904. doi:10.1074/jbc.M110.130781.

Michel M, Dahmann C. Tissue mechanical properties modulate cell extrusion in the *Drosophila* abdominal epidermis. Development. 2020;147(5):dev179606. doi:10.1242/dev.179606.

Mirth CK, Shingleton AW. Integrating body and organ size in *Drosophila*: recent advances and outstanding problems. Front Endocrinol (Lausanne). 2012;3:49. doi:10.3389/fendo.2012.00049.

Miyashita K, Fujii T. Nucleotide sequence and analysis of a gene (chiA) for a chitinase from *Streptomyces lividans* 66. Biosci Biotechnol Biochem. 1993;57(10):1691–1698. doi:10.1271/bbb.57.1691.

Musso G, Costanzo M, Huangfu M, Smith AM, Paw J, San Luis B-J, Boone C, Giaever G, Nislow C, Emili A, *et al.* The extensive and condition-dependent nature of epistasis among whole-genome duplicates in yeast. Genome Res. 2008;18(7):1092–1099. doi:10.1101/gr.076174.108.

Nardi JB, Bee CM, Wallace CL. Remodeling of the abdominal epithelial monolayer during the larva-pupa-adult transformation of Manduca. Dev Biol. 2018;438(1):10–22. doi:10.1016/j.ydbio.2018.03.017.

Ninov N, Chiarelli DA, Martin-Blanco E. Extrinsic and intrinsic mechanisms directing epithelial cell sheet replacement during *Drosophila* metamorphosis. Development. 2007;134(2):367–379. doi:10.1242/dev.02728.

Ninov N, Menezes-Cabral S, Prat-Rojo C, Manjon C, Weiss A, Pyrowolakis G, Affolter M, Martín-Blanco E. Dpp signaling directs cell motility and invasiveness during epithelial morphogenesis. Curr Biol. 2010;20(6):513–520. doi:10.1016/j.cub.2010.01.063.

Nyirkos P, Golds EE. Human synovial cells secrete a 39 kDa protein similar to a bovine mammary protein expressed during the non-lactating period. Biochem J. 1990;269(1):265–268. doi:10.1042/bj2690265.

Osterfield M, Berg CA, Shvartsman SY. Epithelial patterning, morphogenesis, and evolution: *Drosophila* eggshell as a model. Dev Cell. 2017;41(4):337–348. doi:10.1016/j.devcel.2017.02.018.

Osterfield M, Du X, Schupbach T, Wieschaus E, Shvartsman SY. Three-dimensional epithelial morphogenesis in the developing *Drosophila* egg. Dev Cell. 2013;24(4):400–410. doi:10.1016/j.devcel.2013.01.017.

Panzade S, Matis M. The microtubule minus-end binding protein patronin is required for the epithelial remodeling in the *Drosophila* abdomen. Front Cell Dev Biol. 2021;9:682083. doi:10.3389/fcell.2021.682083.

Park JM, Brady H, Ruocco MG, Sun H, Williams D, Lee SJ, Kato T, Richards N, Chan K, Mercurio F, *et al.* Targeting of TAK1 by the NF-kappa B protein relish regulates the JNK-mediated immune response in *Drosophila*. Genes Dev. 2004;18(5):584–594. doi:10.1101/gad.1168104.

Pesch Y-Y, Riedel D, Patil KR, Loch G, Behr M. Chitinases and imaginal disc growth factors organize the extracellular matrix formation at barrier tissues in insects. Sci Rep. 2016;6(1):18340. doi:10.1038/srep18340.

Pinteac R, Montalban X, Comabella M. Chitinases and chitinase-like proteins as biomarkers in neurologic disorders. Neurol Neuroimmunol Neuroinflamm. 2021;8(1):e921. doi:10.1212/NXI.0000000000000921.

Prat-Rojo C, Pouille PA, Buceta J, Martin-Blanco E. Mechanical coordination is sufficient to promote tissue replacement during metamorphosis in *Drosophila*. EMBO J. 2020;39(3):e103594. doi:10.15252/embj.2019103594.

Punia N, Primon M, Simpson GR, Pandha HS, Morgan R. Membrane insertion and secretion of the Engrailed-2 (EN2) transcription factor by prostate cancer cells may induce antiviral activity in the stroma. Sci Rep. 2019;9(1):5138. doi:10.1038/s41598-019-41678-0.

Qureshi AM, Hannigan A, Campbell D, Nixon C, Wilson JB. Chitinase-like proteins are autoantigens in a model of inflammation-promoted incipient neoplasia. Genes Cancer. 2011;2(1):74–87. doi:10.1177/1947601911402681.

Ramesh P, Dey NS, Kanwal A, Mandal S, Mandal L. Relish plays a dynamic role in the niche to modulate *Drosophila* blood progenitor homeostasis in development and infection. Elife. 2021;10:e67158. doi:10.7554/eLife.67158.

Recklies AD, White C, Ling H. The chitinase 3-like protein human cartilage glycoprotein 39 (HC-gp39) stimulates proliferation of human connective-tissue cells and activates both extracellular signal-regulated kinase- and protein kinase B-mediated signalling pathways. Biochem J. 2002;365(1):119–126. doi:10.1042/bj20020075.

Renkema GH, Boot RG, Au FL, Donker-Koopman WE, Strijland A, Muijsers AO, Hrebicek M, Aerts JMFG. Chitotriosidase, a chitinase, and the 39-kDa human cartilage glycoprotein, a chitin-binding lectin, are homologues of family 18 glycosyl hydrolases secreted by human macrophages. Eur J Biochem. 1998;251(1-2):504–509. doi:10.1046/j.1432-1327.1998.2510504.x.

Richardson BE, Lehmann R. Mechanisms guiding primordial germ cell migration: strategies from different organisms. Nat Rev Mol Cell Biol. 2010;11(1):37–49. doi:10.1038/nrm2815.

Rittenhouse KR, Berg CA. Mutations in the *Drosophila* gene *bullwinkle* cause the formation of abnormal eggshell structures and bicaudal embryos. Development. 1995;121(9):3023–3033. doi:10.1242/dev.121.9.3023.

Rossi A, Kontarakis Z, Gerri C, Nolte H, Holper S, Krüger M, Stainier DYR. Genetic compensation induced by deleterious mutations but not gene knockdowns. Nature. 2015;524(7564):230–233. doi:10.1038/nature14580.

Rudrapatna VA, Bangi E, Cagan RL. A Jnk-Rho-Actin remodeling positive feedback network directs Src-driven invasion. Oncogene. 2014;33(21):2801–2806. doi:10.1038/onc.2013.232.

Ryder E, Blows F, Ashburner M, Bautista-Llacer R, Coulson D, Drummond J, Webster J, Gubb D, Gunton N, Johnson G, *et al.* The DrosDel collection: a set of P-element insertions for generating custom chromosomal aberrations in *Drosophila melanogaster*. Genetics. 2004;167(2):797–813. doi:10.1534/genetics.104.026658.

Samac DA, Hironaka CM, Yallaly PE, Shah DM. Isolation and characterization of the genes encoding basic and acidic chitinase in *Arabidopsis thaliana*. Plant Physiol. 1990;93(3):907–914. doi:10.1104/pp.93.3.907.

Sarov M, Barz C, Jambor H, Hein MY, Schmied C, *et al.* A genome-wide resource for the analysis of protein localisation in *Drosophila*. Elife. 2016;5:e12068. doi:10.7554/eLife.12068.

Schimpl M, Rush CL, Betou M, Eggleston IM, Recklies AD, van Aalten Daan MF. Human YKL-39 is a pseudo-chitinase with retained chitooligosaccharide-binding properties. Biochem J. 2012;446(1):149–157. doi:10.1042/BJ20120377.

Shao R, Hamel K, Petersen L, Cao QJ, Arenas RB, Bigelow C, Bentley B, Yan W. YKL-40, a secreted glycoprotein, promotes tumor angiogenesis. Oncogene. 2009;28(50):4456–4468. doi:10.1038/onc.2009.292.

Sharabi K, Hurwitz A, Simon AJ, Beitel GJ, Morimoto RI, Rechavi G, Sznajder JI, Gruenbaum Y. Elevated CO_2 levels affect development, motility, and fertility and extend life span in *Caenorhabditis elegans*. Proc Natl Acad Sci U S A. 2009;106(10):4024–4029. doi:10.1073/pnas.0900309106.

Sharabi K, Lecuona E, Helenius IT, Beitel GJ, Sznajder JI, Gruenbaum Y. Sensing, physiological effects and molecular response to elevated CO2 levels in eukaryotes. J Cell Mol Med. 2009;13(11-12):4304–4318. doi:10.1111/j.1582-4934.2009.00952.x.

Siomava N, Wimmer EA, Posnien N. Size relationships of different body parts in the three dipteran species *Drosophila melanogaster*, *Ceratitis capitata* and *Musca domestica*. Dev Genes Evol. 2016;226(3):245–256. doi:10.1007/s00427-016-0543-6.

Sokac AM, Biel N, De Renzis S. Membrane-actin interactions in morphogenesis: lessons learned from *Drosophila* cellularization. Semin Cell Dev Biol. 2022;133:107–122.

Starz-Gaiano M, Cho NK, Forbes A, Lehmann R. Spatially restricted activity of a *Drosophila* lipid phosphatase guides migrating germ cells. Development. 2001;128(6):983–991. doi:10.1242/dev.128.6.983.

Sutherland TE, Logan N, Ruckerl D, Humbles AA, Allan SM, Papayannopoulos V, Stockinger B, Maizels RM, Allen JE. Chitinase-like proteins promote IL-17-mediated neutrophilia in a tradeoff between nematode killing and host damage. Nat Immunol. 2014;15(12):1116–1125. doi:10.1038/ni.3023.

Swarup S, Verheyen EM. Wnt/Wingless signaling in *Drosophila*. Cold Spring Harb Perspect Biol. 2012;4(6):a007930. doi:10.1101/cshperspect.a007930.

Tharanathan RN, Kittur FS. Chitin—the undisputed biomolecule of great potential. Crit Rev Food Sci Nutr. 2003;43(1):61–87. doi:10.1080/10408690390826455.

Torres EM, Williams BR, Amon A. Aneuploidy: cells losing their balance. Genetics. 2008;179(2):737–746. doi:10.1534/genetics.108.090878.

Tran DH, Berg CA. *Bullwinkle* and *shark* regulate dorsal-appendage morphogenesis in *Drosophila* oogenesis. Development. 2003;130-(25):6273–6282. doi:10.1242/dev.00854.

Tsigkari KK, Acevedo SF, Skoulakis EM. 14-3-3epsilon is required for germ cell migration in *Drosophila*. PLoS One. 2012;7(5):e36702. doi:10.1371/journal.pone.0036702.

Ulmschneider B, Grillo-Hill BK, Benitez M, Azimova DR, Barber DL, Nystul TG. Increased intracellular pH is necessary for adult epithelial and embryonic stem cell differentiation. J Cell Biol. 2016;215(3):345–355. doi:10.1083/jcb.201606042.

Varela PF, Llera AS, Mariuzza RA, Tormo J. Crystal structure of imaginal disc growth factor-2. A member of a new family of growth-promoting glycoproteins from *Drosophila melanogaster*. J Biol Chem. 2002;277(15):13229–13236. doi:10.1074/jbc.M110502200.

Ward EJ, Berg CA. Juxtaposition between two cell types is necessary for dorsal appendage tube formation. Mech Dev. 2005;122(2):241–255. doi:10.1016/j.mod.2004.10.006.

Ward EJ, Zhou X, Riddiford LM, Berg CA, Ruohola-Baker H. Border of Notch activity establishes a boundary between the two dorsal appendage tube cell types. Dev Biol. 2006;297(2):461–470. doi:10.1016/j.ydbio.2006.05.021.

Watanabe T, Kobori K, Miyashita K, Fujii T, Sakai H, Uchida M, Tanaka H. Identification of glutamic acid 204 and aspartic acid 200 in chitinase A1 of *Bacillus circulans* WL-12 as essential residues for chitinase activity. J Biol Chem. 1993;268(25):18567–18572. doi:10.1016/S0021-9258(17)46665-8.

Wieschaus E, Nüsslein-Volhard C. Looking at embryos. In: Roberts DB, editor. Drosophila: A Practical Approach. Oxford, England: IRL Press; 1986. p. 199–227.

Zhang J, Gratchev A, Riabov V, Mamidi S, Schmuttermaier C, Krusell L, Kremmer E, Workman G, Sage EH, Jalkanen S, *et al.* A novel GGA-binding site is required for intracellular sorting mediated by stabilin-1. Mol Cell Biol. 2009;29(22):6097–6105. doi:10.1128/MCB.00505-09.

Zimmerman SG, Merrihew GE, MacCoss MJ, Berg CA. Proteomics analysis identifies orthologs of human chitinase-like proteins as inducers of tube morphogenesis defects in *Drosophila melanogaster*. Genetics. 2017;206(2):973–984. doi:10.1534/genetics.116.199323.

Zurovcova M, Ayala FJ. Polymorphism patterns in two tightly linked developmental genes, Idgf1 and Idgf3, of *Drosophila melanogaster*. Genetics. 2002;162(1):177–188. doi:10.1093/genetics/162.1.177.

Communicating editor: D. Andrew